single or multiple molecules of ubiquitin to a target protein. The ubiquitinated protein is then marked for degradation by the multisubunit 26 S proteasome complex. The proteolytic core of the complex, the 20 S proteasome, contains multiple peptidase activities that include chymotrypsin-like, postglutamyl peptidase or caspase-like and trypsin-like activities. Ubiquitination has been shown to be a pivotal player in regulating a host of cellular processes, including cell cycle control, differentiation, and quality control (22). It is important not only in cellular homeostasis in tissues/organs, including the nervous system, but also in degradation of misfolded and aberrant proteins.

Autophagy is an evolutionally conserved mechanism responsible for the nonselective bulk degradation of long lived proteins and cytoplasmic recycling of organelles during development, tissue homeostasis, and environmental stress such as starvation or amino acid depletion (23, 24). There are three types of autophagy as follows: macroautophagy, chaperone-mediated autophagy, and microautophagy. Among them, macroautophagy (hereafter referred to as autophagy) is the one mediated by the organelle termed autophagosome. Chaperone-mediated autophagy involves the direct translocation of cytosolic proteins across the lysosomal membrane, which requires protein unfolding by chaperone proteins. Microautophagy involves inward invagination of lysosomal membrane, which delivers a small portion of cytoplasm into the lysosomal lumen.

Autophagy begins with the formation of double membrane-bounded autophagosomes (25–27), which then fuse with lysosomes to form autolysosomes. The contents of autolysosomes are finally degraded by acidic lysosomal hydrolases and the degraded products are transported back to the cytoplasm. Autophagy has been shown to play a role in organelle turnover, cancer cell biology, aging, and neurodegenerative disorders (23, 28–30).

In this study, we determined the involvement of UPP and autophagy in processing of the endogenous optineurin in RGC5 cells, a neuronal cell type recently shown to be of mouse origin (31) and an established model for RGCs (31, 32), as well as neuronal rat adrenal pheochromocytoma PC12 cells (33). The processing of overexpressed wild type optineurin and E50K mutant protein was also studied to test the hypothesis that, similar to other neurodegenerative diseases, UPP function is compromised and autophagy is induced with elevated level or mutation of aggregate-prone optineurin.

EXPERIMENTAL PROCEDURES

Cell Lines—RGC5 cells were obtained from the University of Illinois, Chicago, Ophthalmology Departmental Core Facility, deposited by Dr. Paul Knepper (34) and originally from Dr. Neeraj Agarwal, North Texas Health Science Center, Fort Worth, TX (31). PC12 cells were purchased from American Type Culture Collection (Manassas, VA). The cells were cultured in serum-containing complete medium as described previously (18, 35).

In some experiments, RGC5 cells were treated with tumor necrosis factor-α (TNF-α, 100 ng/ml, R & D Systems, Minneapolis, MN) or interferon-γ (IFN-γ, 20 ng/ml, R & D Systems) for 24 h. Both have been shown to elevate the level of optineurin (14, 15, 36). Tetracycline-regulated (Tet-On) wild type optineurin ($OPTN_{WT}$)-green fluorescence protein (GFP)-inducible stable RGC5 cell line was established as described previously (17). Tet-On-inducible E50K optineurin ($OPTN_{E50K}$)-GFP RGC5 cell line was, in addition, created following the same procedures and strategies. The only exception was that the $OPTN_{WT}$-GFP fragment was replaced with $OPTN_{E50K}$-GFP during the first cloning step (17). The cells were maintained in DMEM complete medium with 10% Tet system certified fetal bovine serum (Clontech), essential and nonessential amino acids, and antibiotics. To induce expression of $OPTN_{WT}$-GFP and $OPTN_{E50K}$-GFP, cells were treated for 16 h with doxycycline (DOX, 1 μg/ml) (Clontech) in DMEM complete medium.

DNA Constructs—Optineurin expression vectors pTarget-$OPTN_{WT}$, pTarget-FLAG-$OPTN_{WT}$, p$OPTN_{WT}$-EGFP, p$OPTN_{WT}$-DsRed, as well as pTarget-$OPTN_{E50K}$, p$OPTN_{E50K}$-GFP, and p$OPTN_{E50K}$-DsRed were constructed as described previously (18). Transient transfection was performed using Lipofectamine LTX and Plus reagent (Invitrogen) for 20–48 h according to the manufacturer's protocol.

Western Blotting—To examine the effects of various inhibitors on levels of the endogenous optineurin, RGC5 and PC12 cells in 6-well plates (300,000 cells/well) were treated for 16 h with vehicle dimethyl sulfoxide (DMSO) or H_2O, proteasomal inhibitors lactacystin (LCT, 1 μM) and epoxomicin (5 μM), autophagic inhibitor 3-methyladenine (3-MA, 5 mM), lysosomal inhibitor NH_4Cl (1 mM), or autophagic inducer rapamycin (2 μM). LCT is a proteasomal inhibitor, but it also inhibits enzymes such as cathepsin A. Epoxomicin, on the other hand, is a potent and specific proteasomal inhibitor. 3-MA inhibits class III phosphatidylinositol 3-kinase (PI3K) that is essential for autophagosome formation, as well as other classes of PI3K. It is used as an effective and selective drug to inhibit autophagy degradation. At 5 mM, it has no detectable effects on other proteolytic pathways (27). NH_4Cl is a lysosomotropic weak base that blocks the intralysosomal degradation of macromolecules via inhibition of the acidification of the endosome-lysosome system. It does not affect enzyme activities.

The cells were lysed with lysis buffer (250 mM NaCl, 50 mM Tris/HCl, pH 7.5, 5 mM EDTA, 0.5% Nonidet P-40) supplemented with protease inhibitor mixture (Sigma). Protein concentration was determined by bicinchoninic acid protein assay (Pierce). Total cell lysate was then subjected to SDS-PAGE under reducing conditions. The proteins were transferred to nitrocellulose membrane, and the level of endogenous optineurin was assessed by Western blotting using rabbit anti-C-terminal optineurin (1:1000, Cayman Chemical). The membrane was also immunoblotted with polyclonal anti-glyceraldehyde 3-phosphate dehydrogenase (GAPDH) (1:5000, Trevigen, Gaithersburg, MD) for loading control. Immunoreactive protein bands were detected by chemiluminescence using SuperSignal substrate (Pierce). Densitometry was performed. The band intensity of the endogenous optineurin was normalized to that of GAPDH.

For levels of proteasome regulatory β5 subunit (PSMB5) that is responsible for the chymotrypsin-like activity of the proteasome (37) and an established autophagic marker microtubule-associated protein 1 light chain 3 (LC3) (25), RGC5 and PC12 cells were transfected for 20 h with pTarget empty vector, pTarget-$OPTN_{WT}$, or pTarget-$OPTN_{E50K}$. Total lysate was subject to SDS-PAGE, and levels of PSMB5, LC3, and GAPDH were assessed by immunoblotting using polyclonal rabbit anti-PSMB5 (1:1000, Abcam, Cambridge, MA), monoclonal anti-LC3 (1:1000, Enzo Life Sciences, Farmingdale, NY), and rabbit anti-GAPDH (1:5000).

Immunoprecipitation (IP)—Lysates from RGC5 cells untreated or treated with 1 μM LCT for 16 h were immunoblotted using polyclonal anti-optineurin or monoclonal anti-ubiquitin (1:2000, Biomol, Enzo Life Sciences). Lysates were also immunoprecipitated with rabbit anti-C-terminal optineurin or rabbit normal IgG (negative control) using the Catch and Release kit (Millipore, Billerica, MA). The proteins pulled down were subjected to SDS-PAGE under reducing conditions. The ubiquitinated proteins were detected with mouse anti-ubiquitin antibody.

Fluorescence Microscopy and Immunohistochemistry—RGC5 and PC12 cells were transfected for 20 h with pEGFP-N1 (mock control), $pOPTN_{WT}$-EGFP, or $pOPTN_{E50K}$-EGFP. The cells were subsequently treated for 24 or 48 h with autophagic inhibitor 3-MA (5 mM) or overnight with rapamycin (2 μM). The cells were fixed, and images were acquired.

For immunofluorescence, the cells were fixed after transfection or treatments, and single or double stained with rabbit anti-optineurin (1:100), rabbit anti-PSMB5 (1:100), or rabbit (MBL International, Woburn, MA) or mouse anti-LC3 (1:100). FITC-goat anti-rabbit IgG, Cy3-goat anti-rabbit IgG, or Cy3-goat anti-mouse IgG (1:200, Jackson ImmunoResearch, West Grove, PA) was used as the secondary antibody. The slides were mounted in Vectashield (Vector Laboratories, Burlingame, CA) with 4′,6-diamidino-2-phenylindole (DAPI).

Photography was carried out using a 63× oil objective on an Axioscope (Carl Zeiss MicroImaging, Thornwood, NY) with the aid of Metamorph software (Molecular Devices, Downingtown, PA). In some experiments, confocal microscopic analysis was performed on a Leica SP2 confocal system (Leica Microsystems, Bannockburn, IL) using the Leica confocal software following sequential scanning to minimize the bleed through.

GFP^u Reporter Assay—To visualize the change of proteasome activity by optineurin transfection, a GFP^u reporter plasmid (American Type Culture Collection) was used. It is a designer reporter consisting of a short 16-amino acid degron CL1 (a substrate for UPP) fused to the C terminus of GFP (38, 39). For GFP^u reporter assay, cells co-transfected with GFP^u and pDsRed empty vector (mock control), $pOPTN_{WT}$-DsRed, or $pOPTN_{E50K}$-DsRed for 24 h were examined by confocal microscopy. Images were captured after sequential scanning, and the intensity of green fluorescence in at least 60 red fluorescent-transfected cells was quantified.

Transmission Electron Microscopy—RGC5 cells transfected for 20 h to express GFP, $OPTN_{WT}$-GFP, or $OPTN_{E50K}$-GFP were fixed in 2.5% glutaraldehyde, 2% paraformaldehyde in sodium cacodylate buffer, pH 7.4, postfixed in osmium tetroxide, and embedded in Epon resin. Ultra thin sections (70 nm) were counterstained with uranyl acetate and lead citrate and observed under a JEOL JEM-1220 transmission electron microscope.

For immunogold experiments, inducible cells without or with DOX treatment were fixed at 4 °C in 4% paraformaldehyde, 0.1% glutaraldehyde, in phosphate-buffered saline, pH 7.4, for 2 h and sequentially dehydrated in ethanol solutions and embedded in LR-White resin. Sections (90 nm) mounted on 200-mesh nickel grids were blocked and then incubated with polyclonal anti-GFP (1:100, for wild type or E50K optineurin-GFP) and monoclonal anti-LC3 (1:50). The secondary antibodies used were 25-nm colloid gold-conjugated goat anti-rabbit IgG and 10-nm gold-conjugated goat anti-mouse IgG (1:25, Jackson ImmunoResearch).

Apoptosis Assay—Apoptosis was evaluated by the Biomol CV-caspase 3/7 detection kit (Enzo Life Sciences) that utilizes the fluorophore, cresyl violet, coupled to the C terminus of the optimal tetrapeptide recognition sequences for caspase 3/7, DEVD ($CR(DEVD)_2$). Cleavage of the target sequences by activated enzymes yields red fluorescence throughout the cell, indicative of apoptotic activity. RGC5 and PC12 cells on glass chamber slides were transiently transfected for 48 h to express GFP, or wild type, or E50K optineurin-GFP. Cells were incubated with $CR(DEVD)_2$ for 60 min after treatment with rapamycin for 30 h. The untreated control did not receive rapamycin treatment. The slides were mounted in Vectashield with DAPI, which stained nuclei of all transfected and nontransfected cells.

The total number of DAPI-stained transfected cells (green) and the number of $CR(DEVD)_2$-stained transfectants (displaying both green and red fluorescence) in 20 of randomly selected 10× fields were counted (40). The percentage of caspase 3/7-positive apoptotic cells in ~100 transfectants (number of green and red cells/number of green only cells) was calculated. The experiments were repeated three times. Statistical analysis was performed using Student's *t* tests.

Transgenic Mice—The E50K transgenic mice were generated as described previously (41). All the experiments using mice were performed in accordance with the Association for Research in Vision and Ophthalmology statement for the Use of Animals in Vision Research.

The intraocular pressure of the transgenic mice was measured using an impact-rebound tonometer (Colonial Medical Supply, Franconia, NH) and optical interferometry tonometer (FISO Technologies, Quebec, Canada). Optic disk imaging and light microscopic histopathological examination of the optic nerve were carried out. Paraffin sections of retinal tissues were prepared for TUNEL assay (39). Sections (5 μm) from 12-month-old normal and transgenic mice were deparaffinized and stained in parallel with hematoxylin and eosin, monoclonal anti-TUJ1 (anti-βIII-tubulin, 1:400, Covance, Princeton, NJ) to highlight RGC layer (42), or polyclonal anti-optineurin (1:100), anti-PSMB5 (1:250), or anti-LC3 (1:200). Qdot 655 goat anti-mouse or rabbit IgG (1:100, Invitrogen) was used as the secondary antibody. The slides were mounted

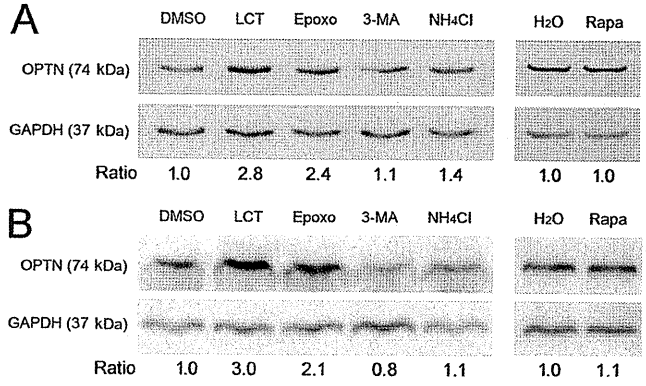

FIGURE 1. **Effects of proteasomal, autophagic, and lysosomal inhibitors on levels of the endogenous optineurin in RGC5 (*A*) and PC12 (*B*) cells.** Cells were treated for 16 h with vehicle DMSO or H_2O, or proteasomal (lactacystin) and epoxomicin (*Epoxo*)), autophagic (*3-MA*), or lysosomal (NH_4Cl) inhibitors. In a separate experiment, cells were also treated with rapamycin (*Rapa*) or vehicle (H_2O) for 16 h. Proteins (25 μg) in cell lysates were immunoblotted with anti-optineurin or anti-glyceraldehyde 3-phosphate dehydrogenase (*GAPDH*). Densitometry was performed. The optineurin/GAPDH relative to the DMSO or H_2O control ratios are presented.

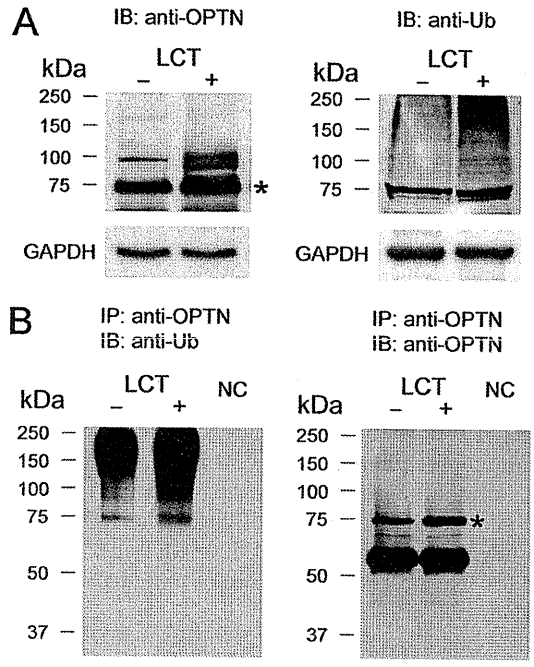

FIGURE 2. *A*, total lysates from RGC5 cells without or with treatment of lactacystin (*LCT*, 1 μM, 16 h) were immunoblotted (*IB*) with polyclonal anti-optineurin (*anti-OPTN, left panel*), anti-GAPDH, or monoclonal anti-ubiquitin (*anti-Ub, right panel*). *B*, total lysates from RGC5 cells without or with the LCT treatment were immunoprecipitated (*IP*) with rabbit anti-OPTN polyclonal antibody or normal rabbit IgG (as a negative control, *NC*) followed by immunoblotting (*IB*) with mouse anti-Ub monoclonal antibody. Optineurin pulldown by rabbit anti-OPTN, but not the rabbit IgG control, showed multiple bands immunoreactive to anti-ubiquitin (*left panel*). The intensity of the ubiquitin-positive bands was enhanced by prior LCT treatment. The same blot was also probed with anti-OPTN (*right panel*) to verify the IP procedure. *, the 74-kDa optineurin band.

in Vectashield, examined under Axioscope, and photographed. In some experiments, sections from 4- and 8-month-old mice were prepared and immunostained with anti-optineurin, anti-PSMB5, and anti-LC3. For EM, 12-month-old mouse eyes were fixed in 2.5% glutaraldehyde, 2% paraformaldehyde in phosphate buffer. The retinas were dissected out and the tissues were postfixed in 1% osmium tetroxide, sequentially dehydrated, and embedded in Spurr's resin. Thin sections (90 nm) were cut and stained for examination under JEOL 1200 EX transmission electron microscope.

RESULTS

Endogenous Optineurin Level in RGC5 and PC12 Cells—Cells were treated with proteasomal, autophagic, and lysosomal inhibitors. As can be seen in Fig. 1, the endogenous optineurin level in both RGC5 and PC12 cells was increased by 2–3-fold upon treatment with proteasomal inhibitors, LCT and expoxomicin, but only by 1.1–1.4-fold with autophagic and lysosomal inhibitors. Rapamycin, an autophagic inducer, did not alter the optineurin level, supporting the 3-MA results that autophagy has a minimal role in the processing of the endogenous optineurin.

Optineurin Is Ubiquitinated—Lysates from RGC5 cells were immunoprobed for optineurin and ubiquitin. Consistent with results from Fig. 1, the level of optineurin was increased upon treatment of LCT. Also seen were higher molecular weight bands with stronger intensities in LCT-treated samples (Fig. 2*A*, *left panel*). Meanwhile, LCT treatment, as anticipated, resulted in an enhanced level of total ubiquitinated proteins in cell lysates (Fig. 2*A*, *right panel*).

Lysates were in addition immunoprecipitated with polyclonal anti-optineurin and immunoprobed with monoclonal anti-ubiquitin. Multiple bands immunoreactive to anti-ubiquitin were observed in the immunoprecipitated protein pool, indicating that the endogenous optineurin in RGC5 cells was ubiquitinated (Fig. 2*B*, *left panel*). The intensity of the ubiquitin-positive bands was enhanced by prior LCT treatment. The same blot was also probed with anti-optineurin to verify the IP procedure (Fig. 2*B*, *right panel*).

Optineurin Foci Formation—After transfection, the overexpressed optineurin-GFP fusion protein distributed diffusely in the cytoplasm of RGC5 and PC12 cells with dots or granular structures observed most notably near the nucleus (Fig. 3). These structures, referred to as foci, were also observed previously in human retinal pigment epithelial and trabecular meshwork cells (18). Foci formation in addition was noted in cells after transfection to overexpress E50K optineurin-GFP. The number and the size of the E50K-GFP foci were greater than those of the wild type (Fig. 3), as was reported previously in retinal pigment epithelial cells (18).

Reduced Proteasome Activity in Optineurin Overexpressing Cells—RGC5 cells transfected for 20 h to express wild type and E50K optineurin-GFP were immunostained for PSMB5 as an indication of proteasome activity (37). The staining intensity in green optineurin-overexpressing RGC5 cells was much reduced compared with mock controls and nontransfected cells (Fig. 4*A*). Western blot analyses indicated that the PSMB5 protein level was decreased (0.36 ± 0.10 and 0.30 ± 0.14, respectively, $n = 3$, $p < 0.002$) as the optineurin level was increased by 8–10-fold upon transfection of pTarget-wild type and E50K optineurin (Fig. 4*B*). Similar alterations were also observed in PC 12 cells (data not shown).

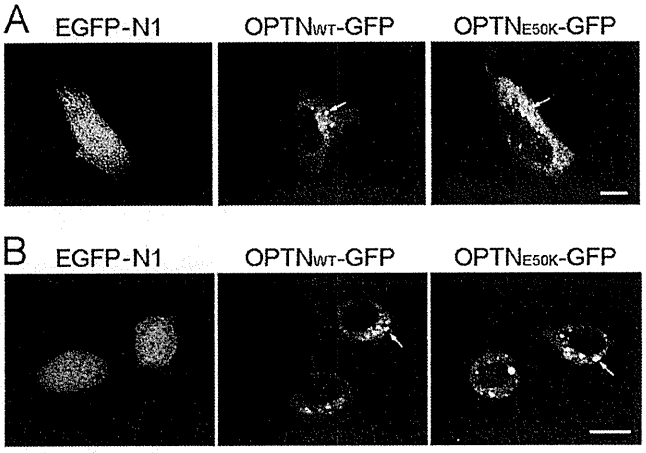

FIGURE 3. **Foci formation in RGC5 (*A*) and PC12 (*B*) cells after 20 h of transfection with pEGFP-N1 (mock control), pOPTN$_{WT}$-GFP, and pOPTN$_{E50K}$-GFP to express GFP, wild type, and E50K optineurin-GFP.** The optineurin-GFP fusion proteins distributed diffusely in the cytoplasm of RGC5 and PC12 cells with dots or granular structures (*arrows*) observed most notably near the nucleus. These structures are referred to as foci. *Scale bar,* 10 μm.

The cells were subsequently co-transfected with pOPTN$_{WT}$-DsRed and GFP^u reporter plasmid. This ubiquitin proteasome system reporter has been shown to be degraded in mammalian cells in an ubiquitin-dependent manner (38, 39). Proteasomal inhibitors such as LCT, but not other protease inhibitors, increased the steady state level of GFP^u (39). Its fluorescence readout and dependence on ubiquitin thus make GFP^u a simple and reliable tool (30). Results shown in Fig. 4, *C* and *D*, revealed that the GFP^u green fluorescence was increased, indicating a lowered proteasome activity in cells transfected with pOPTN$_{WT}$-DsRed compared with those of DsRed control and nontransfected cells. A decreased proteasome activity was also seen in cells transfected with pOPTN$_{E50K}$-DsRed (Fig. 4*C*).

Induction of Autophagy in Optineurin Overexpressing Cells—Following optineurin transfection, RGC5 (Fig. 5) and PC12 (data not shown) cells were stained for the autophagic marker LC3. The intensity of LC3 staining in optineurin-transfected green cells was found stronger than that seen in mock controls and nontransfected cells (Fig. 5*A*). Partial co-

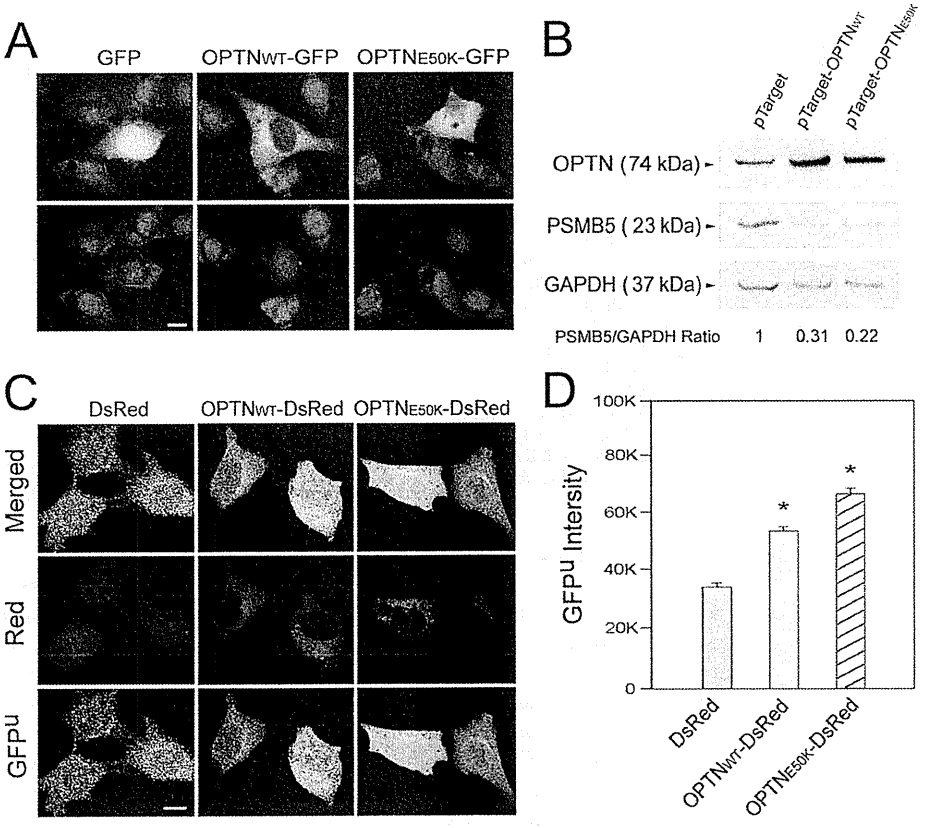

FIGURE 4. *A*, PSMB5 immunostaining (in *red*) in RGC5 cells. The cells were transfected for 20 h to express GFP, OPTN$_{WT}$-GFP, or OPTN$_{E50K}$-GFP. All transfectants displayed green fluorescence. Note a reduced PSMB5 staining intensity in optineurin-GFP-expressing green cells compared with GFP-expressing or nontransfected cells. The reduction was more striking with the E50K mutation than the wild type. *Scale bar,* 10 μm. *B*, Western blotting for PSMB5 protein level. RGC5 cells were transfected for 20 h with pTarget, pTarget-OPTN$_{WT}$, or pTarget-OPTN$_{E50K}$. Total lysate was subject to SDS-PAGE and immunoblotting (*IB*) using polyclonal rabbit anti-optineurin, anti-PSMB5, or anti-GAPDH. The optineurin (*OPTN*) level, normalized to that of GAPDH, was increased by 9.8- and 7.5-fold, respectively, after wild type and E50K optineurin-GFP transfection. The PSMB5/GAPDH relative to the GFP control ratios are presented. Similar results were also obtained with PC12 cells (data not shown). *C*, GFP^u reporter assay. RGC5 cells were co-transfected with GFP^u and pDsRed, pOPTN$_{WT}$-DsRed, or pOPTN$_{E50K}$-DsRed for 20 h. The transfected cells displaying both green and red fluorescence were examined by confocal sequential analyses. The loss of GFP^u green fluorescence is an indication of proteasome activity. The fluorescence intensity from GFP^u is thus inversely correlated to the proteasome activity. *Scale bar,* 10 μm. *D*, intensity of green fluorescence from GFP^u in red fluorescent-transfected cells was quantified. Results are presented as mean ± S.E. ($n > 60$) per transfected cells. The higher the value, the lower is the proteasome activity. *, $p < 0.0001$ compared with DsRed controls.

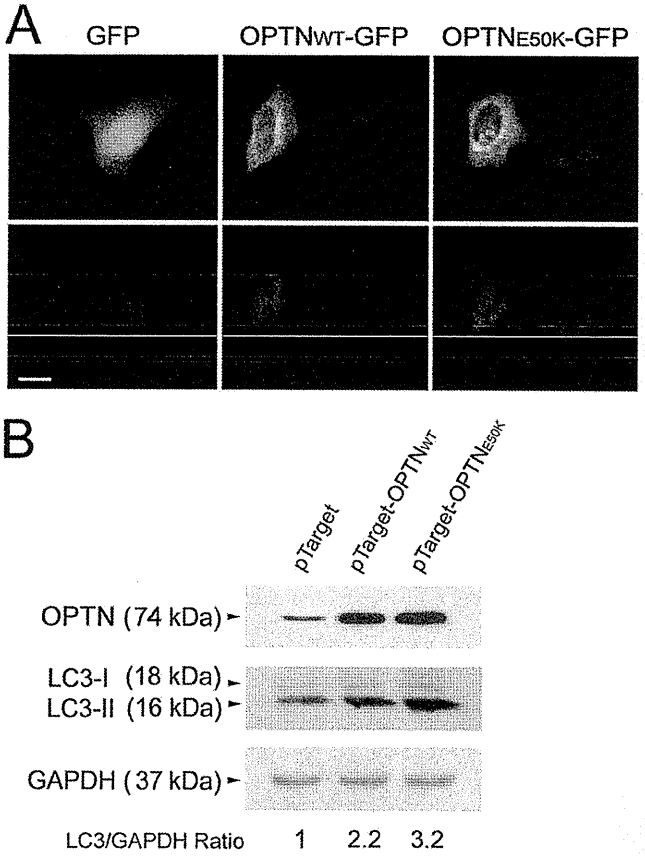

FIGURE 5. *A*, LC3 immunostaining in transfected RGC5 cells. The cells transfected for 20 h to express GFP, $OPTN_{WT}$-GFP, or $OPTN_{E50K}$-GFP were stained with rabbit anti-LC3 in *red*. The GFP and LC3 merged images are presented. Note an increased LC3 staining in optineurin-transfected green cells. The optineurin foci (*green*) and LC3 (*red*) were co-localized partially in the perinuclear region in *yellow*. *Bar*, 10 μm. *B*, Western blotting for LC3 protein level. RGC5 cells were transfected for 20 h with pTarget, pTarget-$OPTN_{WT}$, or pTarget-$OPTN_{E50K}$. Total lysate was subject to SDS-PAGE and immunoblotting (*IB*) using rabbit anti-optineurin, mouse anti-LC3, or rabbit anti-GAPDH. Both LC3-I and LC3-II protein bands were detected. The OPTN level, normalized to that of GAPDH, was increased by 11.5- and 12.3-fold, respectively, after wild type and E50K optineurin transfection. The LC3/GAPDH relative to the pTarget control ratios are presented. Similar alterations were also observed in PC12 cells (data not shown).

localization between optineurin foci and LC3 staining was observed.

LC3 exists in two forms. LC3-I (18 kDa) is cytosolic and LC3-II (16 kDa) is lipidated (conjugated to phosphatidylethanolamine) which is inserted into the membrane. The amount of LC3-II is correlated with the extent of autophagosome formation, and increasing levels of LC3-II on immunoblots have been used to document induction of autophagy (27). In RGC5 cells, the level of LC3 protein, especially the active LC3-II form, was found substantially increased (2.4 ± 0.4 and 2.7 ± 0.5 respectively, $n = 5$, $p < 0.002$) by Western blotting upon overexpression of wild type and E50K optineurin (Fig. 5*B*).

In separate experiments, RGC5 cells were treated with TNF-α and IFN-γ for 24 h. The optineurin level was increased by ~2-fold, as was reported previously (14, 15, 36). Foci formation was not apparent, but the PSMB5 level was found reduced by 40–60%, and the LC3-II level was elevated by 1.9–2.5-fold (Fig. 6). Similar PSMB5 and LC3 alterations were also observed in inducible cell lines when wild type and E50K optineurin-GFP levels were induced by 10–12-fold, and foci were formed upon DOX treatment (data not shown). It is of note that the overexpressed or up-regulated optineurin levels seen in Figs. 4–6 are not the expression levels but rather the stationary state levels set by expression and degradation. The resulting level depends not only on the translational increase but also on the maximum ability of the cell to degrade the excess proteins. This indicates that the transient overexpression might be much higher than 10 times but could be regulated somewhat by the autophagic degradation process.

Furthermore, electron dense as well as electron-light double or multiple membrane autophagosome- and autolysosome-like structures or vesicles (43, 44) were prominently observed by electron microscopy in RGC5 cells after optineurin transfection (Fig. 7*A*, *panels a–c*). These structures were rarely detected in GFP control (Fig. 7*A*, *panel d*) and nontransfected (data not shown) cells.

Autophagosome-like structures were also observed in inducible wild type (data not shown)- and E50K (Fig. 7*B*, *panels a* and *b*)-GFP-expressing cells following DOX induction but not in noninduced cells (Fig. 7*B*, *panel b, inset*). Immunogold studies showed co-localization of E50K optineurin-GFP and LC3 in autophagosome-like structures (Fig. 7*B*, *panels c* and *d*).

Optineurin Foci Formation Is Regulated by Autophagy—RGC5 (Fig. 8, *A* and *B*) and PC12 (data not shown) cells transfected with pOPTN$_{WT}$-GFP and/or pOPTN$_{E50K}$-GFP for 20 h were treated with 3-MA or rapamycin for 24 or 48 h. The 3-MA-treated cells showed more optineurin wild type foci formation compared with the untreated controls (Fig. 8*A*), and the foci enhancement was more dramatically seen at the 48-h time point. The rapamycin-treated cells, on the other hand, showed less foci formation compared with the untreated group in both pOPTN$_{WT}$-GFP and pOPTN$_{E50K}$-GFP transfectants (Fig. 8*B*), suggesting that the overexpressed optineurin was cleared, at least in part, via the autophagy pathway.

Rapamycin Treatment Reduces the Level of Apoptosis Induced by Overexpressed Optineurin—RGC5 (Fig. 8*C*) and PC12 (data not shown) cells were transiently transfected to express GFP alone, wild type or E50K optineurin-GFP followed by treatment of rapamycin. Images were captured, and the percentage of cells that exhibited activated caspase 3/7 enzymes, representing apoptotic activity, in the transfected population was determined. Results indicated that without the rapamycin treatment, the percentage of caspase 3/7-positive cells in total wild type- and E50K optineurin-GFP-overexpressing transfectants was increased by ~1.8–2.5-fold ($p < 0.008$) compared with that in pEGFP-N1-transfected mock controls (Fig. 8*C*). After the rapamycin treatment, the level of apoptosis in optineurin transfectants was declined to within the control limits (Fig. 8*C*).

Transgenic E50K Mouse—The E50K mouse is transgenic, not a knock-in mouse. The transgene was expressed using the chicken β-actin promoter (pCAGGS) with CMV enhancer.

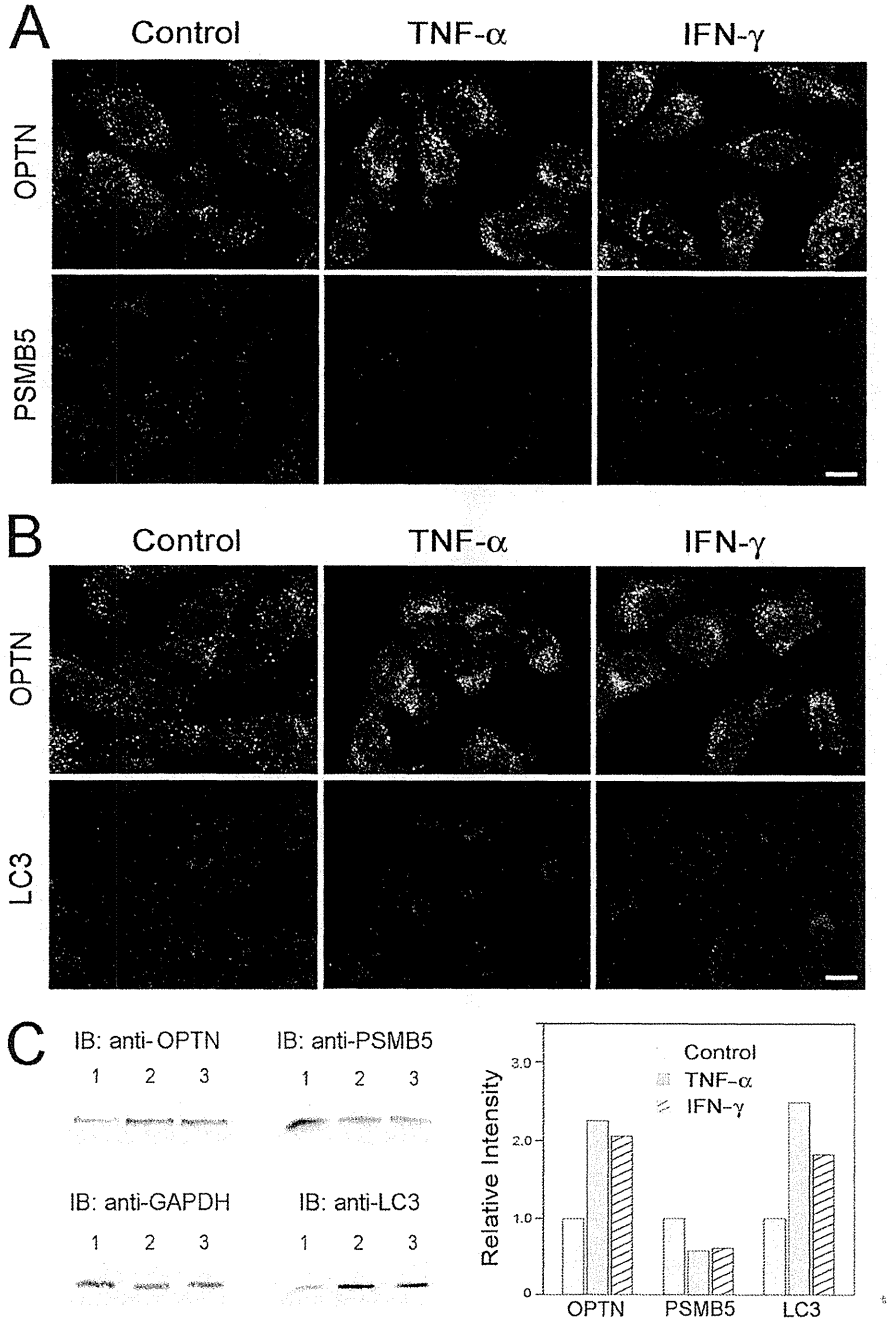

FIGURE 6. *A*, optineurin and PSMB5 immunostaining in RGC5 cells. The cells were treated with TNF-α (100 ng/ml) or IFN-γ (20 ng/ml) for 24 h and were stained with polyclonal rabbit anti-optineurin in *green* or polyclonal rabbit anti-PSMB5 in *red*. The micrographs shown for optineurin and PSMB5 staining were from different specimens. *B*, optineurin and PSMB5 immunostaining in RGC5 cells. The cells were treated with TNF-α or IFN-γ as in *A*. The specimens were double stained with rabbit anti-optineurin in *green* and monoclonal anti-LC3 in *red*. Cells from the same fields are shown for both optineurin and LC3 staining. *Scale bar*, 10 μm. *C*, immunoblotting (*IB*) using anti-optineurin (*OPTN*), anti-PSMB5, anti-LC3, and anti-GAPDH in cells untreated (*lane 1*, control), or treated with TNF-α (*lane 2*) or IFN-γ (*lane 3*) for 24 h. Note that the 18-kDa LC3-I band was barely visible. Only the 16-kDa LC3-II band is shown. As stated earlier, LC3 exists in two forms. LC3-I is cytosolic and LC3-II is lipidated and membrane-bound. The amount of LC3-II is correlated with the extent of autophagosome formation, and an increasing level of LC3-II on immunoblots signals autophagy induction. *Bar graph* depicts the relative intensities (levels) of OPTN, PSMB5, and LC3 compared with untreated controls after normalization to the GAPDH level.

The copy number for the mutant gene was ~12–14 per mouse (41). Although the distribution remained similar, the overall optineurin expression was higher in the retina of E50K transgenic mice compared with the endogenous optineurin expression. The RGC loss and retinal thinning were seen 12 months after birth in the transgenic mice. By 16 months, ~43% of the retinal thickness and ~20% of RGC numbers were reduced (41). Excavation of the optic nerve head was also observed. Apoptotic RGCs were detected in 16- month or older E50K mice. The average intraocular pressure reading for mutant mice was in the normal range of 15 ± 1 mm Hg for all ages examined (41).

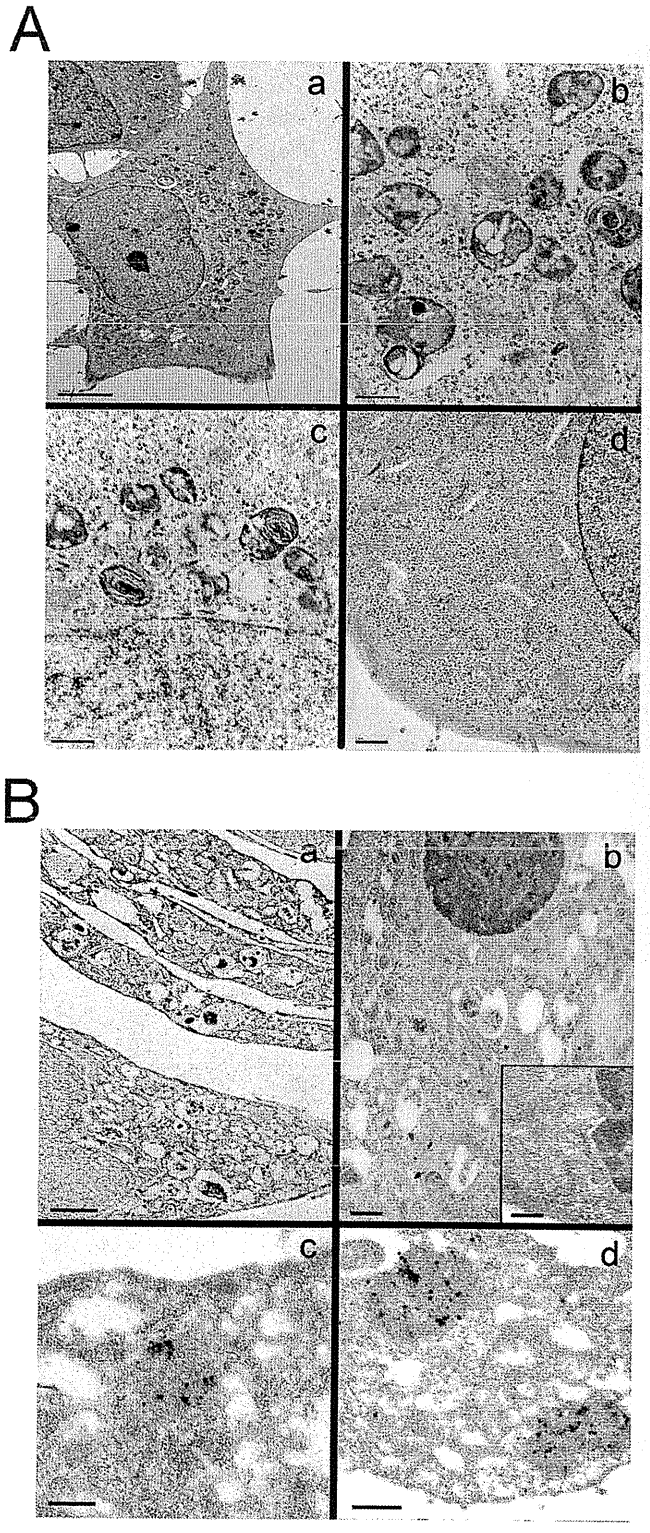

FIGURE 7. *A*, autophagosome- and autolysosome-like structures in optineurin wild type (*panels a* and *b*)- and E50K-GFP (*panel c*)-expressing RGC5 cells. By electron microscopy, the electron dense, organelle-sequestrating, double or multiple membrane structures with diameter averaged between 400 and 600 nm were not observed in GFP-expressing mock-transfected cells (*panel d*). *Scale bar*, 5 μm in *panel a*, 0.5 μm in *panels b* and *c*, and 1 μm in *panel d*. *B*, autophagosome- and autolysosome-like structures are observed in inducible RGC5 cells after DOX induction to express E50K optineurin-GFP (*panels a–d*). A lower magnification micrograph is shown in *panel a* demonstrating those structures in the cytoplasm of several cells. Co-localization of optineurin-GFP (25 nm gold particles) and LC3 (10 nm gold particles) in those structures is seen by immunogold labeling experiments (*panels c* and *d*). The autophagosome- and autolysosome-like structures are barely detected in noninduced controls (*inset* in *panel b*). *Scale bar*, 1 μm in *panel a*, 0.5 μm in *panel b*, and 0.2 μm in *inset*, *panels c* and *d*.

Tissue sections from 12-month-old E50K transgenic mice displayed a fainter staining of PMSB5 but a stronger staining of LC3 in RGCs compared with those from control littermate mice (Fig. 9*B*). Staining with anti-optineurin also yielded a higher intensity in the transgenic tissues as expected (Fig. 9*B*). The enhanced LC3 and reduced PSMB5 staining was also observed in sections from the 4- and 8-month-old transgenic mice (data not shown). Interestingly, no pathology was apparent in the former mice although retinal thickness appeared to be somewhat reduced in the latter.

The staining results in 12-month-old E50K transgenic and normal mice were confirmed by Western blotting of retinal extracts (Fig. 9*C*). By electron microscopy, autophagosome-like structures were demonstrated in RGCs of E50K transgenic eyes (Fig. 9*D*). Quantification analyses indicated that the structures were found in 22 of 33 RGCs examined in transgenic mouse sections, but only in 1 of 23 RGCs in controls.

DISCUSSION

In eukaryotic cells, the ubiquitin-proteasome and autophagy pathways are two major routes for protein clearance (19–21). This study demonstrates that proteasomal inhibition led to an increase in the endogenous optineurin level in neuronal RGC5 and PC12 cells (Fig. 1). On the other hand, autophagic and lysosomal inhibition as well as autophagic activation had little effect. The UPP thus appeared to be the major pathway for endogenous optineurin processing. Autophagy and lysosomes had a rather minor, if any, role. Supporting this conclusion, the endogenous optineurin in RGC5 cells was found ubiquitinated (Fig. 2). UPP has been shown to be the pathway that degrades in a specific manner short lived proteins. The involvement of UPP is therefore consistent with our finding that the half-life of the endogenous optineurin is ~8 h (17). Ubiquitination of the endogenous optineurin also agrees with a previous observation that ^{35}S-labeled, *in vitro*-translated optineurin binds to ubiquitin and is ubiquitinated (16).

Our study further indicates that upon optineurin overexpression or mutation, the proteasome activity in neuronal cells is decreased (Fig. 4) whereas autophagy is induced. The induction of autophagy is evidenced by an increased immunostaining (Fig. 5*A*) for an established autophagic marker LC3 (25), an increased protein level of LC3-II (Fig. 5*B*), the lipidated form of LC3 that inserts into the membrane and correlates with the appearance of LC3-positive autophagosomes (27, 45–47), plus the detection of autophagosome- and autolysosome-like structures in transfected cells (Fig. 6). The overexpressed wild type and E50K optineurins appeared to be processed largely through autophagy, as autophagic activator rapamycin diminishes, whereas the inhibitor 3-MA augments the foci formation (Fig. 8, *A* and *B*).

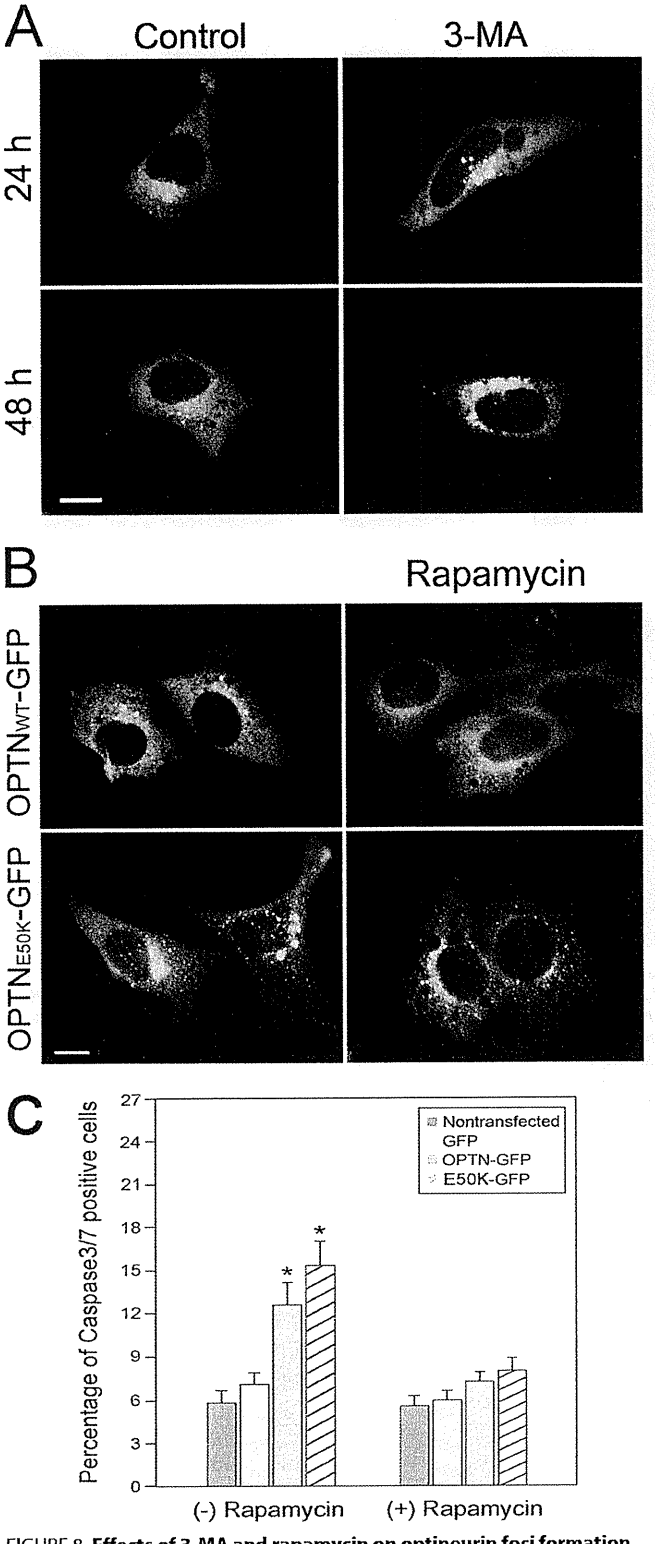

FIGURE 8. **Effects of 3-MA and rapamycin on optineurin foci formation.** *A*, RGC5 cells transfected for 20 h with pOPTN$_{WT}$-GFP were untreated (control) or treated for 24 or 48 h with 3-MA (5 mM), an autophagy inhibitor. Optineurin foci formation was visualized under a Zeiss fluorescence microscope. Note an increased foci formation in 3-MA-treated cells. *B*, RGC5 cells transfected with pOPTN$_{WT}$-GFP and pOPTN$_{E50K}$-GFP were treated for 20 h with rapamycin (2 μM), an autophagy inducer. Note a reduction in foci formation with rapamycin treatment. *Scale bar*, 10 μm. Similar results were also obtained with PC12 cells (data not shown). *C*, percentage of caspase 3/7-positive apoptotic cells in transfected RCG5 cells. The cells transfected for 48 h to express GFP (mock control), wild type optineurin-GFP (OPTN-GFP), and E50K optineurin-GFP (E50K-GFP) were examined by a caspase 3/7 detection kit. One set of cells was treated with 2 μM of rapamycin ((+) *Rapamycin*) for the last 30 h and another was untreated ((−) *Rapamycin*). Images in 20 of 10× fields were captured, and cell counting was performed to determine the total number of transfected cells (*green*) and the number of caspase 3/7-positive transfectants (*green* and *red*). Percentage of caspase 3/7-positive apoptotic transfected cells was calculated. Results from three independent experiments are shown in mean ± S.E. *, $p < 0.008$ compared with GFP controls. Similar patterns were also observed with PC12 cells (data not shown).

A decrease in the PSMB5 level and an increase in the LC3 level were similarly observed in cells treated with TNF-α and IFN-γ (Fig. 6) as well as in inducible cell lines (data not shown). Such *in vitro* changes were likewise observed *in vivo* in E50K transgenic mice. The E50K-overexpressing mice developed phenotype that mimicked the clinical features of NTG patients, including neuropathy of the optic disc and degeneration of the RGCs without an increased intraocular pressure (41). This mouse line thus appears to be the first NTG mouse model. It is notable that the intensity changes of PSMB5 and LC3 staining, although not dramatic, were readily visible (Fig. 9*B*). The protein level changes in the 12-month-old E50K mice were confirmed by Western blotting (Fig. 9*C*). Autophagosome- and autolysosome-like structures were also observed in the E50K specimens (Fig. 9*D*).

It has been documented that when a cytosolic protein is aggregate-prone, it becomes a poor proteasome substrate. One example is α-synuclein, a protein of unknown function and a major component of Lewy bodies (aggregates) observed in Parkinson disease. Mutations of α-synuclein are known to cause autosomal dominant, early onset Parkinson disease. Previous studies have disclosed that both UPP and autophagy are routes for α-synuclein degradation, and that although soluble α-synuclein is cleared by proteasome, the aggregated protein or mutants are preferentially cleared by autophagy (30, 47).

The optineurin degradation hence parallels that described for α-synuclein. The endogenous optineurin seems to be degraded chiefly through the ubiquitin pathway. When optineurin is up-regulated or mutated in neuronal cells, autophagy becomes involved (Figs. 5–7).

The optineurin overexpression characteristics bear similarities to those seen in neurodegenerative diseases, including Alzheimer and Huntington (20, 38, 48). After transfection with wild type or E50K optineurin, the optineurin foci are observed to distribute in the perinuclear region in proximity to the Golgi complex (17, 18, 40). Following precedent of those described for aggresomes, inclusion bodies, or Lewy bodies, the optineurin foci are formed in a microtubule-dependent manner (17, 18). They appear to be LC3-positive (Fig. 5*A*). Also, the proteasome function is impaired (Fig. 4, *C* and *D*) as was seen in neurodegenerative diseases (38, 50, 51). In addition, overexpression of both wild type and E50K optineurin leads to apoptosis in cultured cells (40), and the toxicity can be rescued by rapamycin treatment (Fig. 8*C*). These analogies further underline that glaucoma shares common features with neurodegenerative diseases (52–54).

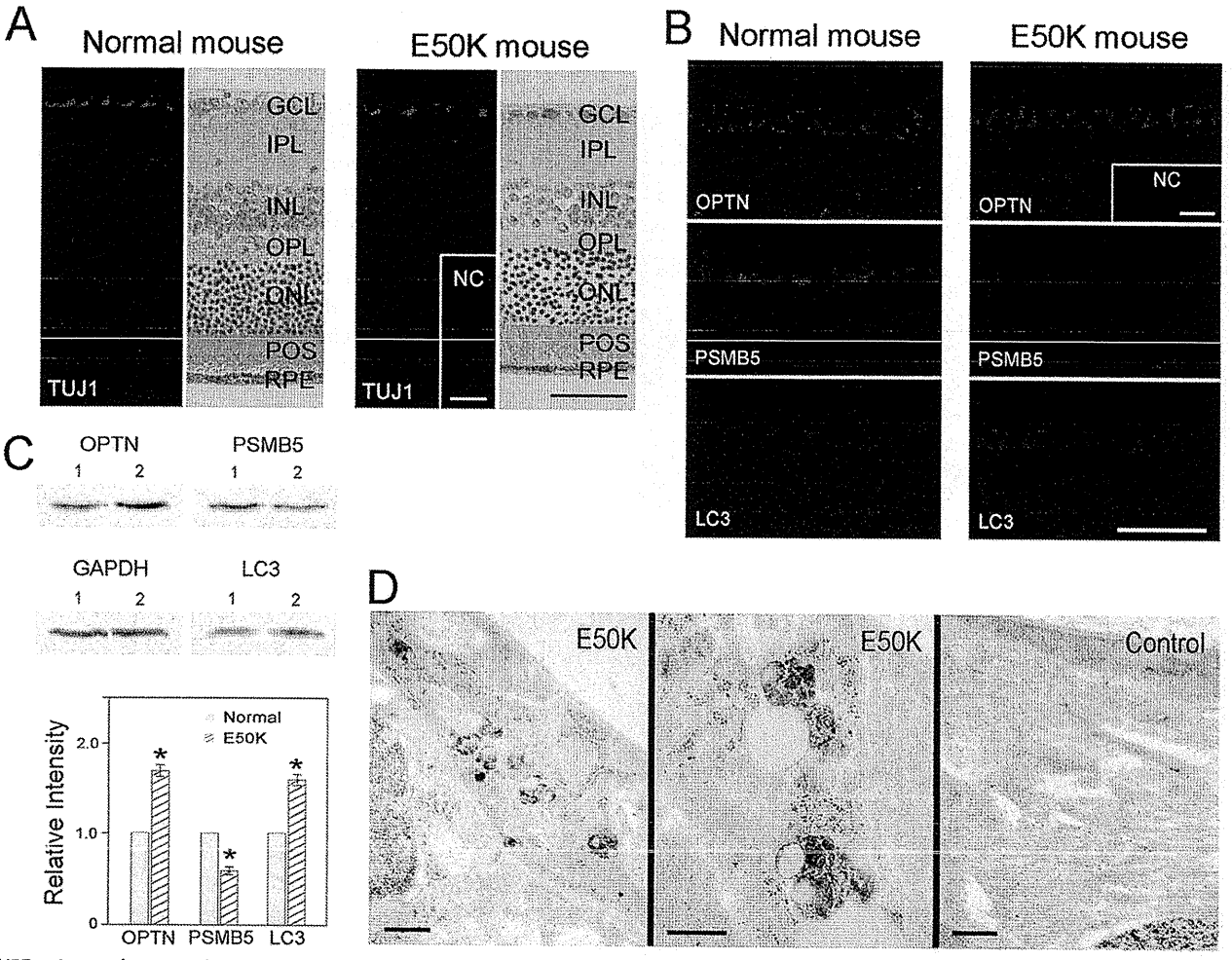

FIGURE 9. *A*, retinal sections from 12-month-old E50K transgenic and normal littermate mice were stained with monoclonal anti-TUJ1 (in *red*) to highlight the RGC layer and with hematoxylin and eosin to demonstrate retinal layers. *GCL*, ganglion cell layer; *IPL*, inner plexiform layer; *INL*, inner nuclear layer; *OPL*, outer plexiform layer; *ONL*, outer nuclear layer; *POS*, photoreceptor outer segments; and *RPE*, retinal pigment epithelium. Note that the retinal thickness is reduced in the E50K transgenic specimen compared with normal control. *Scale bar*, 50 μm. *B*, retinal sections from normal and E50K mice were stained in parallel with polyclonal anti-optineurin, anti-PSMB5, or anti-LC3 (all in *red*). All staining was done using the same antibody concentrations with identical exposure times. As RGCs are the focus of the study, staining in RGCs and the adjacent inner plexiform layer is shown at a higher magnification. Negative controls (*NC*) in which serial sections were stained only with secondary antibodies (for both monoclonal and polyclonal primary antibodies) are shown as *insets*. There was a modest decrease in staining intensity of PSMB5 but an increase in LC3 staining in the RGC layer in transgenic sections compared with normal controls. The optineurin staining was also enhanced in the transgenic mouse. *Scale bar*, 50 μm. *C*, Western blotting for OPTN, PSMB5, LC3, and GAPDH levels in retinal extracts from normal (*lane 1*) or E50K (*lane 2*) mice. Note that for LC3, the 18-kDa LC3-I band was extremely faint. Only the 16-kDa LC3-II band is shown. *Bar graphs*, representing results from three experiments, depict the levels of optineurin, PSMB5, and LC3 relative to normal after normalization to the GAPDH level. *, $p < 0.0053$ compared with normal. *D*, autophagosome- and autolysosome-like structures are observed in RGCs of E50K mouse (*left* and *middle panels*) but are rarely seen in normal littermates (*right panel*). *Bar*, 1 μm in the *left panel*, and 0.5 μm in *middle* and *right panels*.

The role or significance of the foci observed in glaucoma is at present unclear. Interestingly, the roles of inclusion bodies and aggresomes formed in other neurodegenerative diseases are also not clear. As summarized in a number of reviews (21, 26, 55, 56), the inclusion bodies and aggresomes may play a protective role by sequestering toxic, misfolded protein species and providing the cells with an opportunity of delayed protein degradation. They may also inactivate the proteasome and mediate cytotoxicity. Inhibition of proteasome is believed to induce autophagy, which serves as a default mechanism for degradation of the accumulated abnormal proteins. However, when the autophagic clearance system reaches saturation, unable to eliminate the excess proteins, dysregulation or defection may occur, contributing to apoptosis and pathology (26). Supporting this notion, diffuse and abnormal proteins accumulate and aggregate to form inclusions that can disrupt the neural system in Atg5 (autophagy-related gene 5)-deficient mice (57). Also, the protein accumulation and neurodegenerative phenotype could be reverted by activation of the autophagy pathway with a gene therapy approach (58) or infusion of rapamycin (55). It is suggested that there may exist a threshold as a point of divergence between physiological and pathological autophagy (59), and both the physiological and pathological roles of autophagy remain as critically important areas for investigations. Furthermore, inhibition of proteasome function has also been shown to trigger apoptosis (60) depending on cell types and conditions. Defects in the UPP may drive human pathologies, including neurodegenerative

diseases (30), although there have been controversies that still await further clarification (61).

A similar scenario may take place in optineurin-related glaucoma. In this context, it is intriguing that a persistent accumulation of autophagosomes was observed in a recent study (62) in the rat optic nerve following an optic nerve crush injury. The autophagy observed, possibly related to the lesion-induced calcium influx, was thought to be the major pathophysiological mechanism contributing to the ensuing axonal degeneration. It is also of interest that very recently mutations of optineurin are reported to be involved in the pathogenesis of amyotrophic lateral sclerosis (8). Although the role of foci in pathology remains to be precisely defined, an amyotrophic lateral sclerosis case with the E478G optineurin mutation did show optineurin- and ubiquitin-positive cytoplasmic inclusions. Optineurin in addition is linked to Paget disease (9), a condition characterized by focal increases in bone turnover. The osteoclasts in affected bone also contain intranuclear inclusion bodies (63).

There is growing evidence that ubiquitin may be involved in "selective" autophagy (21, 64). It has been shown that ubiquitin-binding receptors such as p62 are required in the process of autophagic clearance of protein aggregates (61, 64). By binding simultaneously to ubiquitin and autophagosome-associated ubiquitin-like LC3, the receptors mediate docking of ubiquitinated protein aggregates to the autophagosome for selective degradation. Optineurin is ubiquitinated, but whether its aggregates are processed through the "selective" autophagy process is currently unknown.

Taken together, this study provides compelling evidence that in normal homeostatic situations, the turnover of endogenous optineurin involves mainly UPP. When optineurin is up-regulated or mutated, the UPP function is compromised, and autophagy comes into play. A decreased PSMB5 level and an induced autophagy were also demonstrated *in vivo* in RGCs of E50K transgenic mice, validating and making relevant the *in vitro* findings.

Optineurin and E50K mutant have been shown to inhibit NF-κB activation (8, 15). Studies from our laboratory reveal that the interaction with Rab8 and transferrin receptor is stronger with the E50K mutant than the wild type optineurin. The mutant also produces a more prominent foci formation (17, 18), more severe fragmentation of the Golgi complex (18), and a higher level of apoptosis (40) than overexpression of the wild type optineurin. Representing a gain-of-function mutation, E50K in addition impairs more dramatically the transferrin trafficking (65). Based on these observations, we surmise that the defective trafficking, deregulated NF-κB signaling, along with fragmentation of the Golgi complex and increased apoptosis may be the underlying bases how the E50K optineurin mutation renders the patients predisposed to the glaucoma pathology. Autophagy, on the other hand, may not be a primary factor in the disease development. This pathway may simply be induced initially as a protective response with buildup of the aggregate-prone mutant protein. Autophagy may contribute to the demise of the cells only when the buildup exceeds the capacity, exacerbating then the disease condition.

It is additionally noteworthy that although the E50K findings have pathological significance, the wild type optineurin overexpression results may also be of physiological relevance. Optineurin, for example, is known to be up-regulated by proinflammatory cytokines TNF-α (14, 36) and IFN (14). Its expression may be heightened to set off adverse consequences upon acute or chronic inflammation and infection. Increases of TNF-α in the retina and the optic nerve head have been associated with glaucomatous conditions (66).

Knowledge of the degradation pathways acting on optineurin can help in the design of novel therapeutic strategies (30). For example, proteasome activity can be promoted by overexpression of proteasome subunit or molecular chaperones, and autophagy can be up-regulated by rapamycin (30), rapamycin plus lithium combination (67), or small molecule autophagy enhancers (49). Future studies will be focused on this translational aspect.

Acknowledgments—We thank Ruth Zelkha for expert imaging and Jack Gibbons, Division of Biological Sciences, for immunogold electron microscopy.

REFERENCES

1. Allingham, R. R., Liu, Y., and Rhee, D. J. (2009) *Exp. Eye Res.* **88,** 837–844
2. Wiggs, J. L. (2007) *Arch. Ophthalmol.* **125,** 30–37
3. Kwon, Y. H., Fingert, J. H., Kuehn, M. H., and Alward, W. L. (2009) *N. Engl. J. Med.* **360,** 1113–1124
4. Wang, N., Chintala, S. K., Fini, M. E., and Schuman, J. S. (2001) *Nat. Med.* **7,** 304–309
5. Rezaie, T., Child, A., Hitchings, R., Brice, G., Miller, L., Coca-Prados, M., Héon, E., Krupin, T., Ritch, R., Kreutzer, D., Crick, R. P., and Sarfarazi, M. (2002) *Science* **295,** 1077–1079
6. Hauser, M. A., Sena, D. F., Flor, J., Walter, J., Auguste, J., Larocque-Abramson, K., Graham, F., Delbono, E., Haines, J. L., Pericak-Vance, M. A., Rand Allingham, R., and Wiggs, J. L. (2006) *J. Glaucoma* **15,** 358–363
7. Aung, T., Rezaie, T., Okada, K., Viswanathan, A. C., Child, A. H., Brice, G., Bhattacharya, S. S., Lehmann, O. J., Sarfarazi, M., and Hitchings, R. A. (2005) *Invest. Ophthalmol. Vis. Sci.* **46,** 2816–2822
8. Maruyama, H., Morino, H., Ito, H., Izumi, Y., Kato, H., Watanabe, Y., Kinoshita, Y., Kamada, M., Nodera, H., Suzuki, H., Komure, O., Matsuura, S., Kobatake, K., Morimoto, N., Abe, K., Suzuki, N., Aoki, M., Kawata, A., Hirai, T., Kato, T., Ogasawara, K., Hirano, A., Takumi, T., Kusaka, H., Hagiwara, K., Kaji, R., and Kawakami, H. (2010) *Nature* **465,** 223–226
9. Albagha, O. M., Visconti, M. R., Alonso, N., Langston, A. L., Cundy, T., Dargie, R., Dunlop, M. G., Fraser, W. D., Hooper, M. J., Isaia, G., Nicholson, G. C., del Pino Montes, J., Gonzalez-Sarmiento, R., di Stefano, M., Tenesa, A., Walsh, J. P., and Ralston, S. H. (2010) *Nat. Genet.* **42,** 520–524
10. Li, Y., Kang, J., and Horwitz, M. S. (1998) *Mol. Cell. Biol.* **18,** 1601–1610
11. Rezaie, T., and Sarfarazi, M. (2005) *Genomics* **85,** 131–138
12. Kroeber, M., Ohlmann, A., Russell, P., and Tamm, E. R. (2006) *Exp. Eye Res.* **82,** 1075–1085
13. De Marco, N., Buono, M., Troise, F., and Diez-Roux, G. (2006) *J. Biol. Chem.* **281,** 16147–16156
14. Schwamborn, K., Weil, R., Courtois, G., Whiteside, S. T., and Israël, A. (2000) *J. Biol. Chem.* **275,** 22780–22789
15. Sudhakar, C., Nagabhushana, A., Jain, N., and Swarup, G. (2009) *PLoS ONE* **4,** e5114
16. Zhu, G., Wu, C. J., Zhao, Y., and Ashwell, J. D. (2007) *Curr. Biol.* **17,** 1438–1443

17. Ying, H., Shen, X., Park, B., and Yue, B. Y. (2010) *PLoS One* **5,** e9168
18. Park, B. C., Shen, X., Samaraweera, M., and Yue, B. Y. (2006) *Am. J. Pathol.* **169,** 1976–1989
19. Glickman, M. H., and Ciechanover, A. (2002) *Physiol. Rev.* **82,** 373–428
20. McCray, B. A., and Taylor, J. P. (2008) *Neurosignals* **16,** 75–84
21. Kirkin, V., McEwan, D. G., Novak, I., and Dikic, I. (2009) *Mol. Cell* **34,** 259–269
22. Mukhopadhyay, D., and Riezman, H. (2007) *Science* **315,** 201–205
23. Mizushima, N. (2007) *Genes Dev.* **21,** 2861–2873
24. Meijer, A. J., and Codogno, P. (2009) *Crit. Rev. Clin. Lab. Sci.* **46,** 210–240
25. Eskelinen, E. L. (2005) *Autophagy* **1,** 1–10
26. Bao, X. H., Naomoto, Y., Hao, H. F., Watanabe, N., Sakurama, K., Noma, K., Motoki, T., Tomono, Y., Fukazawa, T., Shirakawa, Y., Yamatsuji, T., Matsuoka, J., and Takaoka, M. (2010) *Int. J. Mol. Med.* **25,** 493–503
27. Mizushima, N., Yoshimori, T., and Levine, B. (2010) *Cell* **140,** 313–326
28. Levine, B., and Kroeme, G. (2008) *Cell* **132,** 27–42
29. Mizushima, N., Levine, B., Cuervo, A. M., and Klionsky, D. J. (2008) *Nature* **451,** 1069–1075
30. Rubinsztein, D. C. (2006) *Nature* **443,** 780–786
31. Krishnamoorthy, R. R., Agarwal, P., Prasanna, G., Vopat, K., Lambert, W., Sheedlo, H. J., Pang, I. H., Shade, D., Wordinger, R. J., Yorio, T., Clark, A. F., and Agarwal, N. (2001) *Brain Res. Mol. Brain Res.* **86,** 1–12
32. Van Bergen, N. J., Wood, J. P., Chidlow, G., Trounce, I. A., Casson, R. J., Ju, W. K., Weinreb, R. N., and Crowston, J. G. (2009) *Invest. Ophthalmol. Vis. Sci.* **50,** 4267–4272
33. Greene, L. A., and Tischler, A. S. (1976) *Proc. Natl. Acad. Sci. U.S.A.* **73,** 2424–2428
34. Choi, J., Miller, A. M., Nolan, M. J., Yue, B. Y., Thotz, S. T., Clark, A. F., Agarwal, N., and Knepper, P. A. (2005) *Invest. Ophthalmol. Vis. Sci.* **46,** 214–222
35. Park, B. C., Tibudan, M., Samaraweera, M., Shen, X., and Yue, B. Y. (2007) *Genes Cells* **12,** 969–979
36. Vittitow, J., and Borrás, T. (2002) *Biochem. Biophys. Res. Commun.* **298,** 67–74
37. Caballero, M., Liton, P. B., Challa, P., Epstein, D. L., and Gonzalez, P. (2004) *Biochem. Biophys. Res. Commun.* **323,** 1048–1054
38. Bence, N. F., Sampat, R. M., and Kopito, R. R. (2001) *Science* **292,** 1552–1555
39. Bence, N. F., Bennett, E. J., and Kopito, R. R. (2005) *Methods Enzymol.* **399,** 481–490
40. Koga, T., Shen, X., Park, J. S., Qiu, Y., Park, B. C., Shyam, R., and Yue, B. Y. (2010) *Am. J. Pathol.* **176,** 343–352
41. Chi, Z. L., Akahori, M., Obazawa, M., Minami, M., Noda, T., Nakaya, N., Tomarev, S., Kawase, K., Yamamoto, T., Noda, S., Sasaoka, M., Shimazaki, A., Takada, Y., and Iwata, T. (2010) *Hum. Mol. Genet.* **19,** 2606–2615
42. Huang, Y., Li, Z., van Rooijen, N., Wang, N., Pang, C. P., and Cui, Q. (2007) *Exp. Eye Res.* **85,** 659–666
43. Eskelinen, E. L. (2008) *Autophagy* **4,** 257–260
44. Martinez-Vicente, M., Talloczy, Z., Wong, E., Tang, G., Koga, H., Kaushik, S., de Vries, R., Arias, E., Harris, S., Sulzer, D., and Cuervo, A. M. (2010) *Nat. Neurosci.* **13,** 567–576
45. Klionsky, D. J., Cuervo, A. M., and Seglen, P. O. (2007) *Autophagy* **3,** 181–206
46. Mizushima, N., and Yoshimori, T. (2007) *Autophagy* **3,** 542–545
47. Webb, J. L., Ravikumar, B., Atkins, J., Skepper, J. N., and Rubinsztein, D. C. (2003) *J. Biol. Chem.* **278,** 25009–25013
48. Pan, T., Kondo, S., Le, W., and Jankovic, J. (2008) *Brain* **131,** 1969–1978
49. Renna, M., Jimenez-Sanchez, M., Sarkar, S., and Rubinsztein, D. C. (2010) *J. Biol. Chem.* **285,** 11061–11067
50. Mayer, R. J. (2003) *Drugs News Perspect.* **16,** 103–108
51. Ross, C. A., and Pickart, C. M. (2004) *Trends Cell Biol.* **14,** 703–711
52. McKinnon, S. J. (2003) *Front. Biosci.* **8,** s1140–1156
53. Gupta, N., and Yücel, Y. H. (2007) *Curr. Opin. Ophthalmol.* **18,** 110–114
54. Normando, E. M., Coxon, K. M., Guo, L., and Cordeiro, M. F. (2009) *Exp. Eye Res.* **89,** 446–447
55. García-Arencibia, M., Hochfeld, W. E., Toh, P. P., and Rubinsztein, D. C. (2010) *Semin. Cell Dev. Biol.* **21,** 691–698
56. Glick, D., Barth, S., and Macleod, K. F. (2010) *J. Pathol.* **221,** 3–12
57. Hara, T., Nakamura, K., Matsui, M., Yamamoto, A., Nakahara, Y., Suzuki-Migishima, R., Yokoyama, M., Mishima, K., Saito, I., Okano, H., and Mizushima, N. (2006) *Nature* **441,** 885–889
58. Spencer, B., Potkar, R., Trejo, M., Rockenstein, E., Patrick, C., Gindi, R., Adame, A., Wyss-Coray, T., and Masliah, E. (2009) *J. Neurosci.* **29,** 13578–13588
59. Cherra, S. J., 3rd, Dagda, R. K., and Chu, C. T. (2010) *Neuropathol. Appl. Neurobiol.* **36,** 125–132
60. Jana, N. R., Zemskov, E. A., Wang, Gh., and Nukina, N. (2001) *Hum. Mol. Genet.* **10,** 1049–1059
61. Matsuda, N., and Tanaka, K. (2010) *J. Alzheimers Dis.* **19,** 1–9
62. Knöferle, J., Koch, J. C., Ostendorf, T., Michel, U., Planchamp, V., Vutova, P., Tönges, L., Stadelmann, C., Brück, W., Bähr, M., and Lingor, P. (2010) *Proc. Natl. Acad. Sci.* **107,** 6064–6069
63. Ralston, S. H. (2008) *Bone* **43,** 819–825
64. Wong, E., and Cuervo, A. M. (2010) *Nat. Neurosci.* **13,** 805–811
65. Park, B., Ying, H., Shen, X., Park, J. S., Qiu, Y., Shyam, R., and Yue, B. Y. (2010) *PLoS One* **5,** e11547
66. Tezel, G. (2008) *Prog. Brain Res.* **173,** 409–421
67. Sarkar, S., Krishna, G., Imarisio, S., Saiki, S., O'Kane, C. J., and Rubinsztein, D. C. (2008) *Hum. Mol. Genet.* **17,** 170–178

OPEN ACCESS Freely available online

PLoS one

Modeling Retinal Degeneration Using Patient-Specific Induced Pluripotent Stem Cells

Zi-Bing Jin[1,2☯], Satoshi Okamoto[1☯], Fumitaka Osakada[3], Kohei Homma[1], Juthaporn Assawachananont[1], Yasuhiko Hirami[1], Takeshi Iwata[4], Masayo Takahashi[1,5]*

1 Laboratory for Retinal Regeneration, RIKEN Center for Developmental Biology, Kobe, Japan, **2** School of Optometry and Ophthalmology, Eye Hospital, Wenzhou Medical College, Wenzhou, China, **3** Systems Neurobiology Laboratory, The Salk Institute for Biological Studies, La Jolla, California, United States of America, **4** National Institute of Sensory Organs, National Hospital Organization Tokyo Medical Center, Tokyo, Japan, **5** Center for iPS Research and Application, Kyoto University, Kyoto, Japan

Abstract

Retinitis pigmentosa (RP) is the most common inherited human eye disease resulting in night blindness and visual defects. It is well known that the disease is caused by rod photoreceptor degeneration; however, it remains incurable, due to the unavailability of disease-specific human photoreceptor cells for use in mechanistic studies and drug screening. We obtained fibroblast cells from five RP patients with distinct mutations in the *RP1*, *RP9*, *PRPH2* or *RHO* gene, and generated patient-specific induced pluripotent stem (iPS) cells by ectopic expression of four key reprogramming factors. We differentiated the iPS cells into rod photoreceptor cells, which had been lost in the patients, and found that they exhibited suitable immunocytochemical features and electrophysiological properties. Interestingly, the number of the patient-derived rod cells with distinct mutations decreased *in vitro*; cells derived from patients with a specific mutation expressed markers for oxidation or endoplasmic reticulum stress, and exhibited different responses to vitamin E than had been observed in clinical trials. Overall, patient-derived rod cells recapitulated the disease phenotype and expressed markers of cellular stresses. Our results demonstrate that the use of patient-derived iPS cells will help to elucidate the pathogenic mechanisms caused by genetic mutations in RP.

Citation: Jin Z-B, Okamoto S, Osakada F, Homma K, Assawachananont J, et al. (2011) Modeling Retinal Degeneration Using Patient-Specific Induced Pluripotent Stem Cells. PLoS ONE 6(2): e17084. doi:10.1371/journal.pone.0017084

Editor: Mark Mattson, National Institute on Aging Intramural Research Program, United States of America

Received October 28, 2010; **Accepted** January 15, 2011; **Published** February 10, 2011

Funding: This study was supported by the grant from the Ministry of Health, Labour and Welfare, Japan (#H21-Nanchi-Ippan-216). The funders had no role in study design, data collection and analysis, decision to publish, or preparation of the manuscript.

Competing Interests: The authors have declared that no competing interests exist.

* E-mail: mretina@cdb.riken.jp

☯ These authors contributed equally to this work.

Introduction

Retinitis pigmentosa (RP) leads inevitably to visual impairment due to irreversible retinal degeneration, specifically of primary rod photoreceptors. The condition causes night blindness and visual field defects. The disease onset spans a wide range of ages, but RP most often occurs in late life. There is no treatment that allows patients to avoid deterioration of visual function. RP encompasses a number of genetic subtypes, with more than 45 causative genes and a large number of mutations identified thus far. The genetic heterogeneity of RP suggests a diversity of disease mechanisms, which remain largely unclear. Furthermore, for many of the RP subtypes, no appropriate animal models are available. Although large clinical trials have been conducted with α-tocopherol and β-carotene, these studies found no statistically significant change of visual function in RP patients [1,2]. The underlying mutations causing disease in the patients tested in the clinical trials were not revealed, and the variability of individual responses to these drugs is unknown. One of the reasons why these clinical trials failed to examine the effectiveness of drugs is that the effect of a drug may be different between patients with different underlying mutations.

Induced pluripotent stem (iPS) cells reprogrammed from somatic cells [3,4] have enabled us to easily generate patient-derived terminally differentiated cells *in vitro* [5–7]. We have successfully induced differentiation of photoreceptor cells from both human embryonic stem (ES) cells [8] and iPS cells [9,10]. Modeling pathogenesis and treatment *in vitro* using patient iPS cell-derived photoreceptors will elucidate disease mechanisms; circumvent problems related to differences among species that arise when using animal models; decrease patient risk; and reduce the cost of early-stage clinical trials. Here, we generated iPS cells from RP patients with different mutations and demonstrated the potential of patient-derived photoreceptors for disease modeling.

Materials and Methods

RP patients and genetic mutations

The protocol of this study adhered to the tenets of the Declaration of Helsinki. The study was approved by the ethical committees of the Institute of Biomedical Research and Innovation Hospital and the RIKEN Center for Developmental Biology, Japan. Written informed consent from all patients was obtained. We selected five RP patients from four families whose disease-causing mutations have been identified (**Fig. 1A–D and Fig. S1**). Of the five RP patients in this study, three late-onset patients carried the following mutations: 721Lfs722X in *RP1*, W316G in *PRPH2*, and G188R in *RHO*. Two relatively early-onset patients from the same family carried a H137L mutation in *RP9*, which we

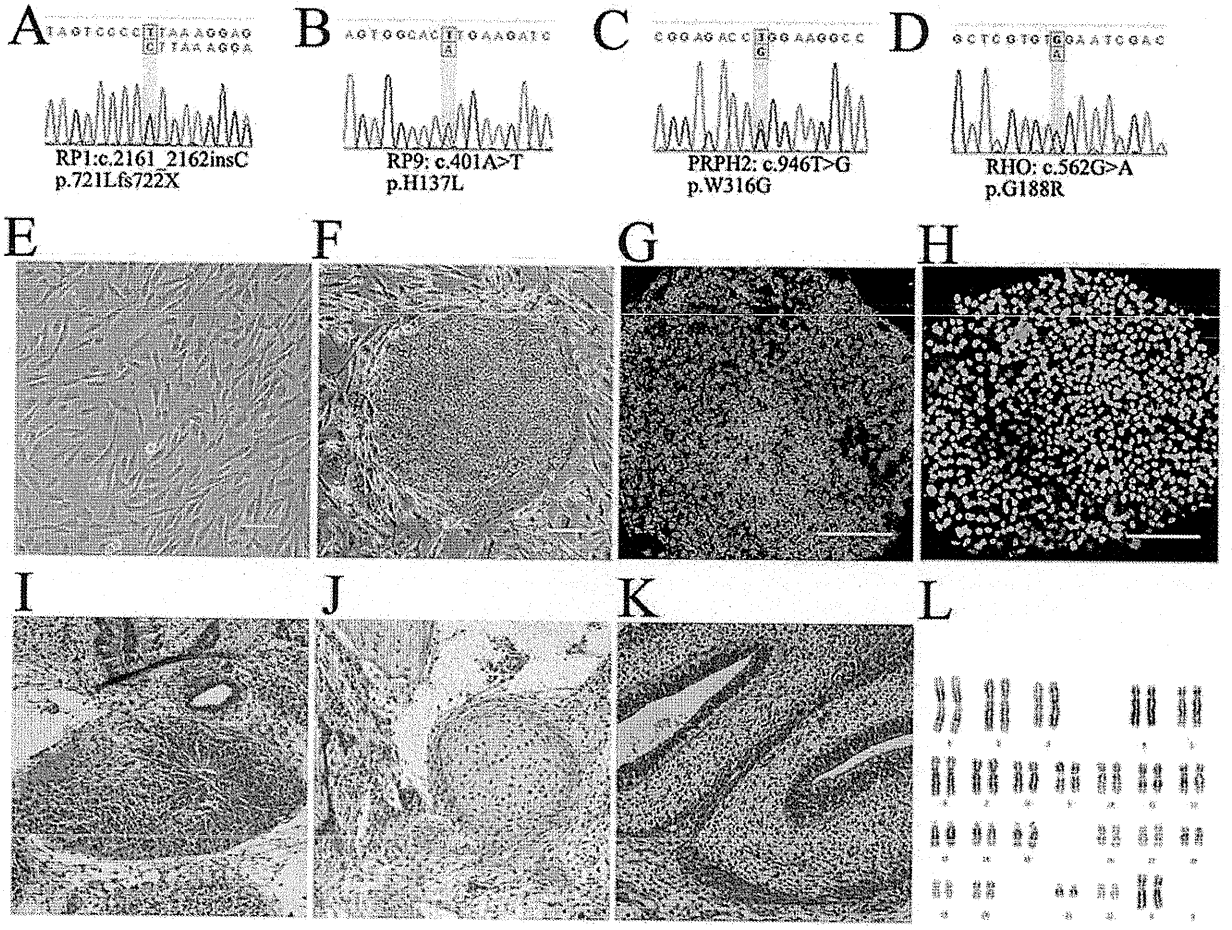

Figure 1. iPS cells derived from RP patients. Mutations identified in patients K21 (RP1) (**A**), K11 and K10 (RP9) (**B**), P101 (PRPH2) (**C**), and P59 (RHO) (**D**). Patient-derived fibroblast cells (**E**) were reprogrammed into iPS cells (**F**). The iPS cells expressed SSEA-4 (**G**) and Nanog (**H**). A teratoma formation test confirmed iPS cells' ability to generate all three germ layers: endoderm (**I**), mesoderm (**J**) and ectoderm (**K**). Karyotype analysis (**I**). Scale bars, 50 μm.
doi:10.1371/journal.pone.0017084.g001

confirmed by both genomic and cDNA sequencing (**Fig. S2**). All patients showed typical manifestations of RP (**Tab. S1**). Peripheral blood obtained from patients was used for DNA isolation. A comprehensive screening of disease-causing genes was carried out as described previously [11]. For the RP9 mutation, total RNA was isolated from fresh blood samples and iPS cells, and synthesized cDNA was subjected to PCR and direct sequencing to confirm whether the mutation was located in the *RP9* gene or the pseudo-RP9 gene (paralogous variant). Both fibroblast and iPS cells were analyzed to re-confirm the identified mutation.

iPS cells generation

To generate iPS cells, retroviral transduction of Oct3/4, Sox2, Klf4, and c-Myc into patient-derived fibroblast cells was carried out as described previously [3]. Established iPS cell lines were maintained on a feeder layer of mitomycin C-treated SNL cells (a murine-derived fibroblast STO cell line expressing the neomycin-resistance gene cassette and LIF) in a humidified atmosphere of 5% CO_2 and 95% air at 37°C. Cells were maintained in DMEM-F12 supplemented with 0.1 mM non-essential amino acids, 0.1 mM 2-mercaptoethanol, 2 mM L-glutamine, 20% KnockOut Serum Replacement (KSR), and 4 ng/ml basic fibroblast growth factor (Upstate Biotechnology).

Transgene quantification

To examine the copy number of transgenes integrated into the host genome, DNA was isolated and quantitative detection of viral transgenes was performed using real-time PCR. The endogenous gene was used as a control. Before quantitative PCR, a standard curve for each primer and/or probe set was determined using a set of plasmid DNA dilutions. Taqman qPCR to detect integrated OCT3/4, KLF4, and MYC was performed using 20 μl reactions consisting of 10 μl TaqMan Master Mix with uracil N-glycosylase, 4.9 μM primers, 250 nM probe, and 1 μl of the DNA sample. Quantification of viral SOX2 was assayed using SYBR Green.

Teratoma formation

Animal protocols were approved by the RIKEN Center for Developmental Biology ethical committee (No. AH18-05). A total of 10^7 trypsinized iPS cells were injected subcapsularly into the testis of SCID mice (two mice per iPS cell line). Four weeks later, the testis was fixed and sectioned for H&E staining.

Immunocytochemistry

Cells were fixed with 4% paraformaldehyde for 15 min at 4°C and then permeabilized with 0.3% Triton X-100 for 45 min. After 1 h blocking with 5% goat serum, cells were incubated with primary antibodies overnight at 4°C and subsequently with secondary antibodies for 1 h at room temperature. The primary and second antibodies used are listed in **Tab. S2**.

Karyotype analysis

Karyotype analysis of the iPS cell chromosomes was carried out using a standard G-band technique (300–400 band level).

Photoreceptor differentiation and drug testing

In vitro differentiation of rod photoreceptor cells was performed as previously reported [8], but with a minor modification. To find a KSR optimal for retinal differentiation, lot testing was conducted before differentiation. iPS colonies were dissociated into clumps with 0.25% trypsin and 0.1 mg/ml collagenase IV in PBS containing 1 mM $CaCl_2$ and 20% KSR. Feeder cells were removed by incubation of the iPS cell suspension on a gelatin-coated dish for 1 h. iPS clumps were moved to a non-adhesive MPC-treated dish (NUNC) in maintenance medium for 3 days, in 20% KSR-containing differentiation medium (DMEM-12 supplemented with 0.1 mM non-essential amino acids, 0.1 mM 2-mercaptoethanol, 2 mM L-glutamine) for 3 days, then in 15% KSR-containing differentiation medium for 9 days, and finally in 10% KSR-containing medium for 6 days. Cells were treated with Lefty-A and Dkk-1 during floating culture. At day 21, the cells were plated en bloc on poly-D-lysine/laminin/fibronectin–coated 8-well culture slides (BD Biocoat) at a density of 15–20 aggregates/cm^2. The cells were cultured in 10% KSR-containing differentiation medium until day 60. Cells were further treated with 100 nM retinoic acid (Sigma) and 100 µM taurine (Sigma) in photoreceptor differentiation medium (GMEM, 5% KSR, 0.1 mM non-essential amino acids, 0.1 mM 2-mercaptoethanol, 1 mM pyruvate, N2 supplement, and 50 units/ml penicillin, 20 µg/ml streptomycin). Differentiated cells from both normal and patient iPS cells were treated with 100 µM α-tocopherol, 200 µM ascorbic acid and 1.6 µM β-carotene starting at differentiation day 120. One week later, cells were fixed for immunostaining.

Electrophysiological recording

Recombinant lentiviral vectors expressing GFP under the control of the Nrl or RHO promoters were generated in HEK293t cells (RIKEN Cell Bank), and differentiated cells were infected with virus on day 90. Cells expressing GFP were targeted for patch clamp recordings. Voltage-clamp recordings were performed with 12–15 MΩ glass electrodes. Signals were amplified using Multiclamp 700B amplifiers (Molecular Devices). The internal solution was 135 mM K-gluconate, 10 mM HEPES, 3 mM KCl, 0.2 mM EGTA, 2.5 mM $MgCl_2$, 5 mM adenosine 5′-triphosphate, 0.3 mM guanosine-5′-triphosphate, 0.06 mM Alexa Fluor 594 (Molecular probes), adjusted to pH 7.6 with KOH. The retinal cells were perfused with oxygen-bubbled external medium: 23 mM $NaHCO_3$, 0.5 mM KH_2PO_4, 120 mM NaCl, 3.1 mM KCl, 6 mM Glucose, 1 mM $MgSO_4$, 2 mM $CaCl_2$, and 0.004% Phenol red. The medium was heated to 37°C with a temperature controller (Warner Instruments).

Cell count and statistical analysis

Differentiated cells visualized with specific antibodies were counted blindly by an independent observer. Data are expressed as means ± s.e.m. The statistical significance of differences was determined by one-way ANOVA followed by Tukey's test or Dunnett's test, or by two-way ANOVA followed by Bonferroni test using the GraphPad Prizm software. Probability values less than 0.05 were considered significant.

Results

Generation of iPS cell lines from patients with RP

Mutations identified in the five patients were confirmed by bi-directional sequencing (**Fig. S1**). Through genotyping of four patients and two normal relatives in the RP9 family, we found the H137L mutation in the *RP9* gene co-segregated with the disease, strongly indicating that the mutation is indeed the genetic cause of the disease. We cultured fibroblasts from skin samples of these patients on gelatin-coated dishes (**Fig. 1E**) and infected them with retroviral vectors encoding *OCT3/4* (also known as *POU5F1*), *SOX2*, *KLF4*, and *c-MYC*, using a previously established method [3]. Each mutation was re-confirmed in both fibroblasts and iPS cells. Established iPS colonies showed human embryonic stem cell-like morphology (**Fig. 1F and Fig. S3A**) and expressed pluripotency markers (**Fig. 1C–D**). We selected iPS cell lines for each patient using multiple criteria. First, we excluded iPS cell lines in which spontaneous differentiation occurred repeatedly during maintenance (**Fig. S3B**). We chose iPS colonies that maintained morphologies similar to those of human ES cells through more than 10 passages. Second, we quantified the transgene copy number and selected iPS cell lines with the fewest integrations, as the risk of gene disruption through random insertion increases with the number of transgenes (**Fig. S4A–E**). Third, in order to select iPS cell lines with full pluripotency, we verified the ability to form teratomas. Teratomas formed by injecting iPS colonies into the testis *in vivo* showed contributions to all three embryonic germ layers: ectoderm, mesoderm, and endoderm (**Fig. 1E–G**). Finally, karyotype analysis was carried out to examine the chromosome integrity. The patient-iPS cells showed normal karyotypes after extended passage, indicating chromosomal stability (**Fig. 1H**). These results provide *in vitro* and *in vivo* functional proof of pluripotency for RP patient-derived iPS cells.

Generation of patient-specific retinal photoreceptor

We previously demonstrated *in vitro* differentiation of retinal photoreceptor cells from wild-type human ES [8] and iPS cells [9,10] using a stepwise differentiation method known as serum-free culture of embryoid body-like aggregates [12]. We first evaluated the differentiation efficiency of three selected iPS cell lines of the five patients (**Fig. 2A**). Retinal progenitor, photoreceptor precursor, retinal pigment epithelium (RPE) and rod photoreceptor cells were sequentially induced (**Fig. 2B–K**), consistent with our previous studies [8–10,12]. All patient-derived iPS cell lines differentiated into RPE cells that form ZO-1+ tight junctions on differentiation day 60, with timing, morphology, and efficiency similar to that of wild-type iPS cells (**Fig. 2D–E; Fig. S5**). Immature photoreceptors expressing Crx and Recoverin (day ~60) were observed as clusters in the colonies (**Fig. S6A–B**). The patient-iPS cells also differentiated into blue Opsin+ or red/green Opsin+ cone photoreceptor cells (**Fig. 2H** and data not shown). Immunostaining of Rhodopsin (a marker of mature rod photoreceptors) revealed no Rhodopsin+ cells at differentiation day 100 (data not shown). Rhodopsin+ cells appeared at differentiation day 120 with a stable efficiency of the three independent iPS cell lines from each patient (**Fig. 2K,N and Fig. S6C**). Additionally, 15.1±0.60% and 13.3±1.65% cells were positive for Recoverin (a conventional marker for both rod, cone photoreceptors and cone bipolar cells) in K21- and K11-iPS cells, respectively

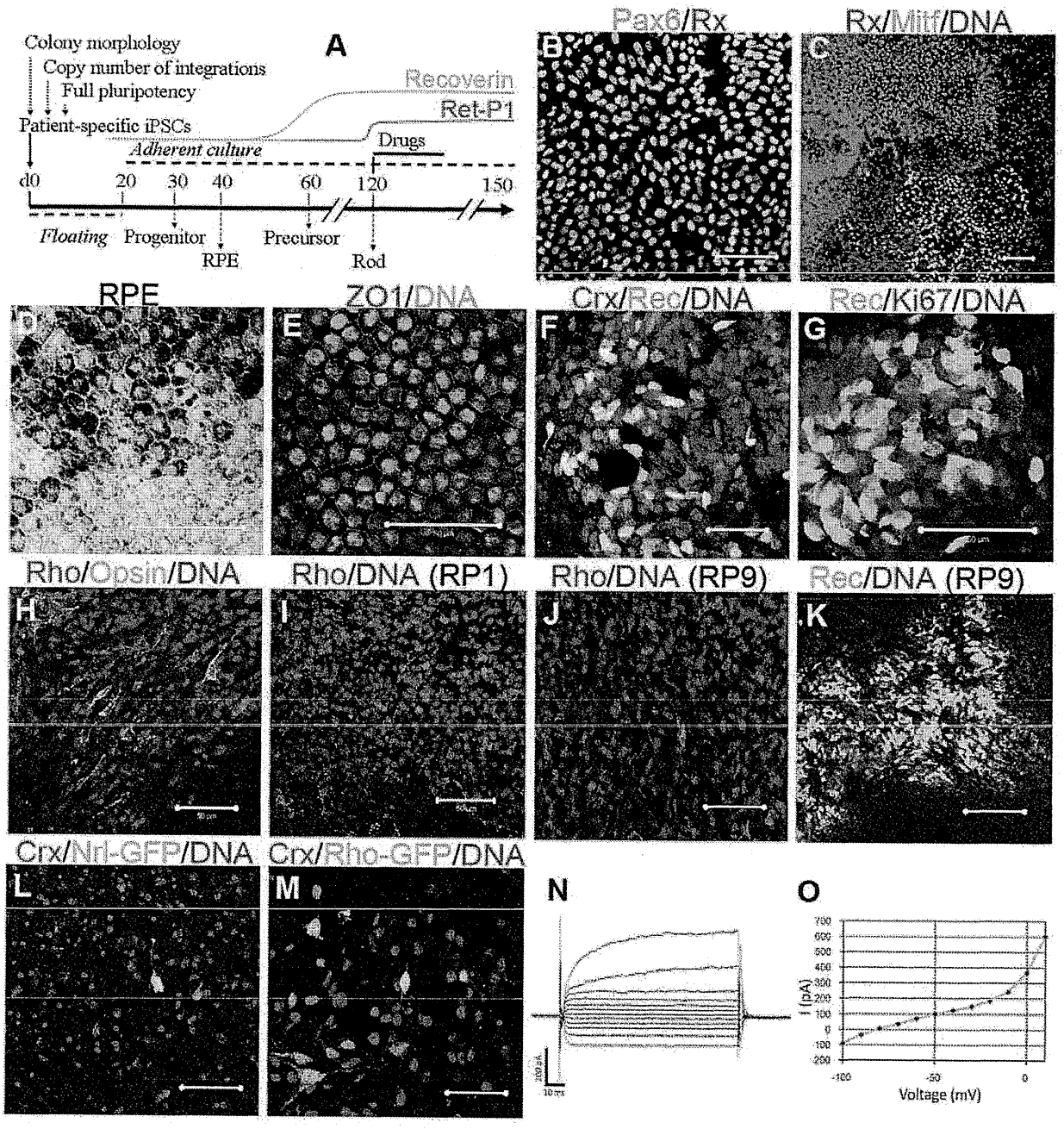

Figure 2. Induction of patient-specific retinal photoreceptor cells. Retinal cells were induced sequentially by *in vitro* differentiation. (**A**) Experimental schema. (**B**) Neural retina progenitor cells (Pax6+Rx+) and RPE progenitor cells (Mitf+) were separated in the culture dish (**C**). Patient-specific RPE cells exhibited hexagonal morphology and pigmentation (**D**) and expressed the tight junction marker ZO-1 (**E**). Photoreceptor cells were positive for immature photoreceptor markers Crx and Recoverin on day 60 (**F**). Recoverin+ cells did not co-express Ki67, a proliferating cell marker (**G**). Differentiation of rod photoreceptors (Rhodopsin+) and cone photoreceptors (Opsin+) from patient iPS cells (**H**). Rhodopsin + rod photoreceptors induced from K21-iPS at day 120 (**I**). K11-derived rod photoreceptors were observed at day 120 (**J**). No Rhodopsin+ cells were detected, but Recoverin+ cells were present at day 150(**K**). Induced rod photoreceptor cells (Crx+) labeled with lentiviral vectors encoding GFP driven by a rod photoreceptor-specific promoter Nrl (**L**: Nrl-GFP) or Rhodopsin (**M**: Rho-GFP). Arrows indicate cells co-expressing Crx and GFP. (**N**) Whole-cell recording of rod photoreceptor cell differentiated human iPS cells. Recorded cells expressed GFP under the control of the Rhodopsin promoter. (**O**) Relationship between voltage and membrane current (i) produced a non-linear curve, suggesting that voltage-dependent channels exist in iPS cell-derived rod photoreceptors Rec, Recoverin; Rho, Rhodopsin. Scale bars, 50 μm.
doi:10.1371/journal.pone.0017084.g002

(data from three selected lines), consistent with stable differentiation. Furthermore, we confirmed rod induction by labeling with lentiviral vectors driving GFP from the Rhodopsin and Nrl promoters, either of which is specifically expressed in rod photoreceptors (**Fig. 2L–M**). Whole-cell patch-clamp recording demonstrated that the rod photoreceptor cell membrane contains voltage-dependent channels, suggesting that differentiated patient-derived rod cells are electrophysiologically functional (**Fig. 2N–O**). Meanwhile, the excluded iPS cell lines (ones that showed spontaneous differentiation during maintenance, or had a high copy number of transgenes), demonstrated a significant diversity of differentiation (**Fig. S7**). Together, these data show that patient-derived iPS cells can differentiate into cells that exhibit many of the immunochemical and electrophysiological features of mature rod photoreceptor cells.

Patient-specific rod cells undergo degeneration *in vitro*

As compared with normal iPS cells, there is no significant difference in rod cell differentiation efficiency at day 120 in K21(RP1)-, P101(PRPH2)-, and P59(RHO)-iPS cell lines (**Fig. 3**). iPS cells from both K11(RP9) and K10(RP9) carried a RP9 mutation; however, rod cell number was significantly lower than in normal iPS cells (**Fig. 3**). We asked whether early death of precursor cells leads to a smaller number of mature rod photoreceptor cells. To determine whether genetic mutations induce degeneration in photoreceptors cells *in vitro*, we extended the culture period and evaluated the number of rod photoreceptors at day 150. In differentiated iPS cells from patient K21(RP1) at day 150, the number of Rhodposin+ cells was significantly decreased (**Fig. 3**). For the K11-iPS cells, no Rhodposin+ cells were found at day 150 (**Fig. 3**). Importantly, some K11-cells at day 150 were positive for Recoverin (10.3±1.99%) and Crx, markers for the rod, cone photoreceptors, and/or bipolar cells (**Fig. 2K** and data not shown), strongly suggesting that cone photoreceptor and/or bipolar cells survived, whereas the rod photoreceptors underwent degeneration *in vitro*. In addition, we detected cells positive for Islet1 (a marker for retinal amacrine, bipolar and ganglion cells), again consistent with the survival of other types of retinal cells (**Fig. S6F**). From these results, we concluded that mature rod photoreceptors differentiated from patient iPS cells selectively degenerate in an RP-specific manner *in vitro*.

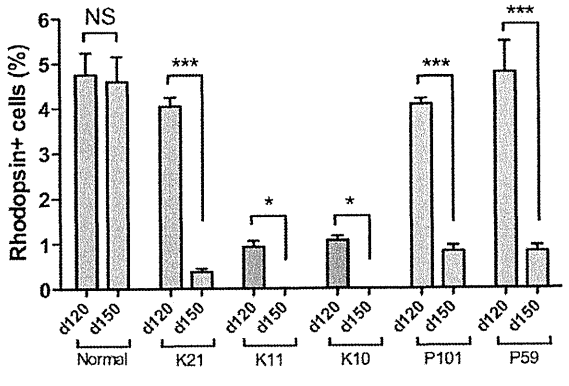

Figure 3. RP patient-derived rod photoreceptors undergo degeneration *in vitro*. iPS cells were differentiated into Rhodopsin+ rod photoreceptors in serum-free culture of embryoid body-like aggregates (SFEB culture). The percentages of Rhodopsin+ rod photoreceptors were evaluated at both day 120 and day 150, respectively. Data were from three independent iPS cell lines derived from the patients. ANOVA followed by Dunnett's test. * $p<0.05$; *** $p<0.001$. Values in the graphs are means and s.e.m.
doi:10.1371/journal.pone.0017084.g003

Cellular stresses involved in patient-derived rod cells

We next asked how the patient-derived rod photoreceptors degenerate. We evaluated apoptosis and cellular stresses in each cell line at both day 100 and day 120, respectively. Interestingly, in the RP9-iPS (K10 and K11) cells, a subset of Recoverin+ cells co-expressed cytoplasmic 8-hydroxy-2'-deoxyguanosine (8-OHdG), a major oxidative stress marker, indicating the presence of DNA oxidation in RP9 patient-derived photoreceptors by differentiation day 100 (**Fig. 4A** and **Fig. S8**). More caspase-3+ cells were presented in the Crx+ photoreceptor cluster of RP9-iPS than in those from other lines (**Fig. 4C–D**). After maturation of the rod photoreceptors from RP9-iPS cells, Rhodopsin+ cells co-expressed Acrolein, a marker of lipid oxidation (**Fig. 4E**), while no Rhodopsin+/Acrolein+ cells were observed in iPS cells derived from other patients carrying different mutations or in normal iPS cells (**Fig. 4F**). This pattern was similar to the cases of 8-OHdG and activated caspase-3. Thus, we conclude that oxidation is involved in the RP9-rod photoreceptor degeneration.

In differentiated RHO-iPS (P59) cells, we found that Rhodopsin proteins were localized in the cytoplasm (**Fig. 4G**), as determined by immunostaining with anti-Rhodopsin antibody (Ret-P1). This pattern is unlike the normal localization of Rhodopsin at the cell membrane in photoreceptors derived from normal iPS or other patient-derived iPS cells (**Fig. 4H** and data not shown). This result suggests accumulation of unfolded Rhodopsin, as reported previously in rhodopsin mutant mice cells [13]. We next examined the possible involvement of endoplasmic reticulum (ER) stress in RHO-iPS cell line degeneration. The Rhodopsin+ or Recoverin+ cells co-expressed immunoglobulin heavy-chain binding protein (BiP) or C/EBP homologous protein (CHOP), two conventional markers of endoplasmic reticulum (ER) stress, from day 120 (**Fig. 4I,K and Fig. S9**), while cells derived from control iPS or other mutant iPS cells were negative for BiP and CHOP (**Fig. 4J,L**). Taken together, these results demonstrate that ER stress is involved in rod photoreceptors carrying a RHO mutation.

Drug evaluation in patient-specific rod cells

The antioxidant vitamins α-tocopherol, ascorbic acid, and β-carotene have been tested in clinical trials as dietary therapies for RP [2] and in another major retinal degenerative disease, age-related macular degeneration [14]. Thus far, mostly due to the lack of appropriate validation models, there has been no evidence supporting the beneficial effects of these compounds on rod photoreceptors. We therefore assessed the effects of these agents on rod photoreceptors derived from patient iPS cells. In mouse retinal culture, short-term treatment with α-tocopherol, ascorbic acid and β-carotene at 100 μM, 200 μM and 1.6 μM, respectively, exerted no significant toxic effects on rod photoreceptor cells (**Fig. S10**). Since the differentiated rod photoreceptors underwent degeneration after day 120, we treated the cells for 7 days with these agents starting at day 120 (**Fig. 2A**). α-Tocopherol treatment significantly increased the number of Rhodopsin+ cells in iPS cells derived from K11- and K10-iPS with the RP9 mutation, while it had no significant effects on iPS cells with the either the RP1, PRPH2 or RHO mutation (**Fig. 5**). In contrast, neither ascorbic acid nor β-carotene treatment had any effect on iPS cells of any genotype (**Fig. S11**). We cannot currently explain the discrepancy between the effects of these antioxidants. It has been reported that under certain circumstances, anti-oxidants can act as "pro-oxidants" [15]. Taken together, our results indicate that treatment with α-tocopherol is beneficial to RP9-rod photoreceptor survival, and causes different effects on Rhodposin+ cells derived from different patients.

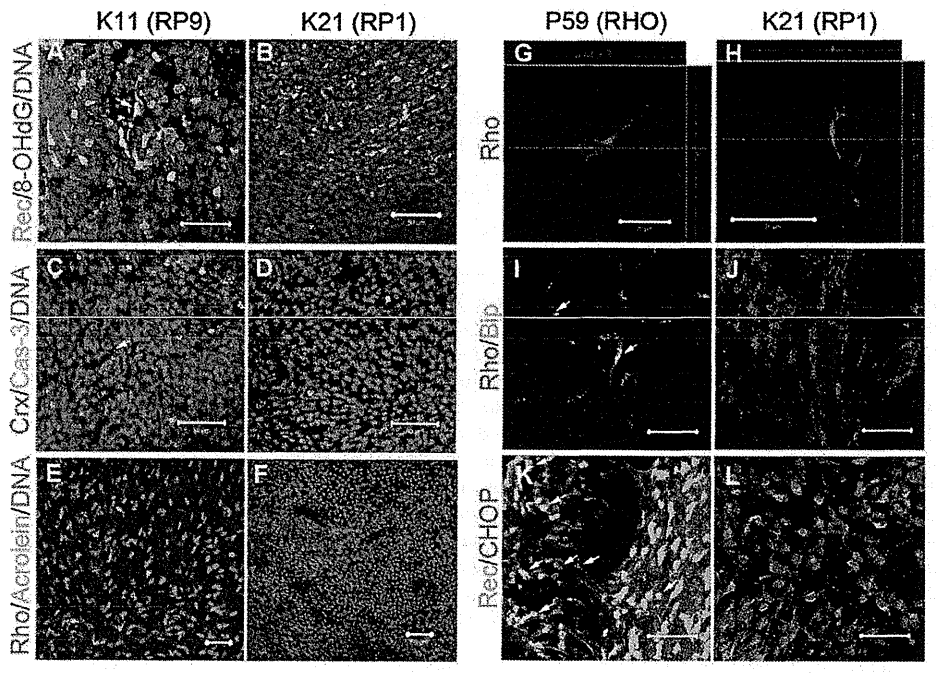

Figure 4. Cellular stress in patient-derived rod photoreceptor cells. Oxidative stress and apoptosis in differentiated rod photoreceptor cells derived from RP9-iPS (**A,C,E**) and RP1-iPS (**B,D,F**). (**A**) 8-OHdG, a marker for DNA oxidation, was found in K11- or K10-iPS–derived differentiated cells (day 100), but not in K21-iPS (**B**). Arrow indicates a cell double-positive for 8-OHdG and Recoverin. (**C**) The number of activated Caspase-3+ cells was greater in K11-iPS differentiation than in K21-iPS (**D**). From day 120, rod photoreceptor cells (Rhodopsin+) derived from RP9-iPS co-expressed the oxidative stress marker Acrolein (**E**); whereas RP1-iPS derivatives did not (**F**). (**G–L**) Abnormal cellular localization of Rhodopsin proteins and endoplasmic reticulum stress in RHO-iPS–derived rod photoreceptors. High magnification revealed cytoplasmic localization of Rhodopsin in rod photoreceptor cells carrying a RHO mutation (**G**) and a normal localization in the cell membrane in K21 cells (**H**). Rod cells derived from RHO-iPS co-expressed the ER stress markers BiP (**I**) and CHOP (**K**). K21-iPS–derived rod cells did not express BiP (**J**) or CHOP (**L**). Arrows indicate double-positive cells. Rec, Recoverin; Rho, Rhodopsin. All scale bars are 50 μm except for G and H (20 μm).
doi:10.1371/journal.pone.0017084.g004

Discussion

By using patient-derived iPS cells and *in vitro* differentiation technology, we have shown that RP9-retinitis pigmentosa is involved, at least in part, in oxidative stress pathways; this has not been reported previously in any animals or cell models. Furthermore, we have demonstrated that the antioxidant α-tocopherol exerts a beneficial effect on RP9-rod cells. Additionally, we have clearly shown that rod photoreceptors derived from patients with a RHO mutation are associated with ER stress; this is

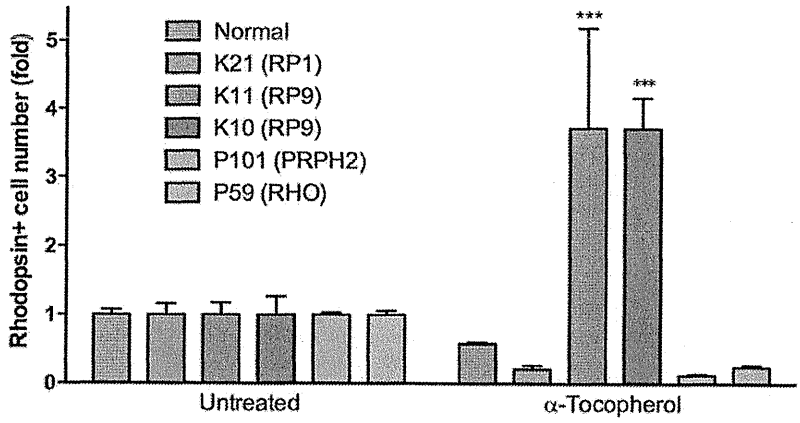

Figure 5. Disease modeling of patient-derived rod photoreceptor cells. α-Tocopherol treatment of patient-specific rod photoreceptors yielded a significant beneficial effect in RP9 mutant cells. Two-way ANOVA Bonferroni post-test showed no significance in other group (n = 3–8). Data represent 1–2 selected iPS cell lines of each patient. ***$p<0.001$. Values in the graphs are means and s.e.m.
doi:10.1371/journal.pone.0017084.g005

the first report of ER stress in a cell culture model for human rod cells. These cell models will be very useful for disease mechanism dissection and drug discovery. By screening several drugs that had already been tested in RP patients, we have revealed that rod photoreceptor cells derived from RP patients with different genetic subtypes exhibit significant differences in drug responses. Among the different types of antioxidants, α-tocopherol has either beneficial or non-beneficial effects on diseased photoreceptors, depending on the genetic mutation. This is the first report of the utilization of iPS cells related to personalized medicine, which will be helpful for routin clinical practice. Our results also provided evidence that genetic diagnosis is essential for optimizing personalized treatment for patients with retinal degenerative diseases [11]. An important future study made possible by this work is the screening of a compound library for drugs that could be used to treat RP. Patient-derived iPS cells revealed differences in pathogenesis and the efficacy of antioxidants among patients with different disease-causing mutations. Although the microenvironment affects the pathogenesis of diseases, and *in vitro* evaluation is not perfect, this study suggests that iPS cells could be used to select between multiple available treatments, allowing physicians to advise each patient individually. The weakness of our method for disease modeling is that differentiation requires a long period of time. Shortening the induction period and identifying appropriate surface markers for rod cells will improve disease modeling using patient-specific iPS cells.

In brief, we generated pluripotent stem cells from retinitis pigmentosa patients and induced them into retinal cells. Compared with normal cells, patient-derived rod cells simulated the disease phenotype and exhibited different responses to specific drugs. We found that patient-specific rod cells underwent degeneration *in vitro*, which maybe related to different cellular stresses. To our knowledge, this is the first report of disease modeling of retinal degeneration using patient-derived iPS cells.

Supporting Information

Figure S1 Pedigrees of K21 (A), P59 (B), K10 and K11 (C). Families of P59 (**B**) and K10 and K11 (**C**) show autosomal dominant mode of inheritance. (**C**) Mutation analysis was performed in four patients and two normal relatives in the RP9 family. The H137L mutation in RP9 gene was co-segregated with the disease in the family. Closed symbols indicate individuals with RP and open symbols indicate unaffected subjects. Question marks indicate symptom unknown. The bars above the symbols indicate examined subjects. Arrow, proband; slash, deceased.
(TIF)

Figure S2 Mutation in the *RP9* gene. (**A**) Alignment of RP9 sequence and pseudo-gene shows the same nucleotide in the mutated location. (**B**) Sequence chromatogram of cDNA sequence demonstrates the c.410A>T (H137L) mutation in the *RP9* gene, instead of the paralogous variant in pseudo-gene which was documented in RetNet (www.sph.uth.tmc.edu/retnet/disease.htm).
(JPG)

Figure S3 Selection by colony morphology. (**A**) iPS colony (K21S4) shows ES-like morphology. (**B**) Spontaneous differentiation in the colony during maintenance (K21S14). Scale bars, 50 μm.
(TIF)

Figure S4 Quantification of transgene copy number. Total copy number of four transgenes in the selected iPS lines. Selected iPS cells with fewest integrations and two high copy number lines used for *in vitro* differentiation.
(TIF)

Figure S5 Efficiency of RPE induction in patient-iPS cells. RPE production of the five patient-iPS cells showed no significant differences ($n = 4$). Data represent the percentage of RPE area at differentiation day 60. One-way ANOVA followed by Dunnett's test. Values are mean and s.e.m.
(TIF)

Figure S6 Induced retinal cells from patient iPS cells (K21S4). Crx+ photoreceptor precursor cells present in the cell cluster on differentiation day 60 (A). Crx+ cells co-expressed Recoverin, indicating differentiation into photoreceptor cells (B). Rhodopsin+ cells had a long process at day 150 (C). In the differentiated cells, we also observed cells positive of PKCα (a marker for bipolar cells) (D). Cells positive for Math5 and Brn3b (markers for ganglion progenitor or ganglion cells (day 60) (E). Cells positive for Islet-1 (a marker for amacrine, bipolar and ganglion cells) (F). Scale bars, 50 μm (A, D, E, and F); 20 μm (B and C).
(TIF)

Figure S7 Differentiation of the patient-iPS cells. iPS colony was cut into uniform sized pieces (**A**) and subjected to a floating culture (P59M8, day 20) (**B**). RPE (pigmented) and recoverin+ (green) cells were efficiently induced (P59M8, day 60) (**C**). (**D**) An excluded iPS line, P59M16, with high number transgenes showed a striking lentoid formation during the floating culture (day 20). Scale bars, 50 μm.
(TIF)

Figure S8 Oxidative stress in photoreceptor cells with the RP9 mutation (K11). (A) Recoverin, (B) 8-OHdG, (C) Recoverin/8-OHdG, (D) Recoverin/8-OHdG/DNA. Arrows indicate cells with weak Recoverin signal positive for 8-OHdG; Arrowheads represent cells with strong Recoverin signal positive for 8-OHdG; Asterisks represent Recoverin+ cells negative for 8-OHdG. Scale bar, 50 μm.
(JPG)

Figure S9 ER stress in photoreceptor cells with the RHO mutation (P59). (A) CHOP, (B) Recoverin, (C) Recoverin/CHOP, (D) Recoverin/CHOP/DNA. Arrows indicate cells with weak Recoverin signals positive for CHOP in nuclei; Arrowheads represent cells with strong Recoverin signals positive for CHOP; Asterisks represent Recoverin+ cells negative for CHOP. Scale bar, 50 μm.
(JPG)

Figure S10 Toxicity testing of the antioxidants in murine retina-derived rod photoreceptor cells. Primary culture of mouse retinal cells treated with 100 μM α-tocopherol, 200 μM ascorbic acid or 1.6 μM β-carotene for 24 hours and the rod photoreceptors were counted using flow cytometry. Value represents the ratio of treated-rod photoreceptors compared with control cells. $n = 4$. One-way ANOVA followed by Dunnett's test. Values are mean and s.e.m. NS, not significant.
(JPG)

Figure S11 Differentiated rod cells from normal and patient iPS cells treated with 200 μM ascorbic acid or 1.6 μM β-carotene did not show statistically significant differences. Two-way ANOVA Bonferroni post-test. Values are mean and s.e.m.
(JPG)

Table S1 Phenotypic data of the RP patients. M, male; F, female; AD, age at diagnosis; BCVA, best corrected visual acuity; HM, hand motion.
(DOC)

Table S2 Antibodies used in the present study.
(DOC)

Acknowledgments

We thank C. Ishigami and Y. Tada for assistance of mutation screening; K. Iseki, N. Sakai, Y. Wataoka, K. Sadamoto, A. Tachibana, C. Yamada for technical assistance; Y. Arata, W. Meng, C. Li, A. Suga, M. Mandai and all members in the Takahashi lab for advice.

Author Contributions

Conceived and designed the experiments: ZBJ MT. Performed the experiments: ZBJ SO FO KH JA. Analyzed the data: ZBJ SO FO. Contributed reagents/materials/analysis tools: MT YH TI. Wrote the paper: ZBJ MT.

References

1. Weleber RG, Gregory-Evans K (2006) Retinitis Pigmentosa and Allied Disorders. In: Hilton DR, Schachat AP, Ryan SJ, eds. Retina. Elsevier Mosby. pp 395–498.
2. Berson EL, Rosner B, Sandberg MA, Hayes KC, Nicholson BW, et al. (1993) A randomized trial of vitamin A and vitamin E supplementation for retinitis pigmentosa. Arch Ophthalmol 11: 761–772.
3. Takahashi K, Tanabe K, Ohnuki M, Narita M, Ichisaka T, et al. (2007) Induction of pluripotent stem cells from adult human fibroblasts by defined factors. Cell 131: 861–872.
4. Yu J, Vodyanik MA, Smuga-Otto K, Antosiewicz-Bourget J, Frane JL, et al. (2007) Induced pluripotent stem cell lines derived from human somatic cells. Science 318: 1917–1920.
5. Park IH, Arora N, Huo H, Maherali N, Ahfeldt T, et al. (2008) Disease-specific induced pluripotent stem cells. Cell 134: 877–886.
6. Raya A, Rodríguez-Pizà I, Guenechea G, Vassena R, Navarro S, et al. (2009) Disease-corrected haematopoietic progenitors from Fanconi anaemia induced pluripotent stem cells. Nature 460: 53–59.
7. Yamanaka S (2007) Strategies and new developments in the generation of patient-specific pluripotent stem cells. Cell Stem Cell 1: 39–49.
8. Osakada F, Ikeda H, Mandai M, Wataya T, Watanabe K, et al. (2008) Toward the generation of rod and cone photoreceptors from mouse, monkey and human embryonic stem cells. Nat Biotechnol 26: 215–224.
9. Osakada F, Jin ZB, Hirami Y, Ikeda H, Danjyo T, et al. (2009) In vitro differentiation of retinal cells from human pluripotent stem cells by small-molecule induction. J Cell Sci 122: 3169–3179.
10. Hirami Y, Osakada F, Takahashi K, Okita K, Yamanaka S, et al. (2009) Generation of retinal cells from mouse and human induced pluripotent stem cells. Neurosci Lett 458: 126–131.
11. Jin ZB, Mandai M, Yokota T, Higuchi K, Ohmori K, et al. (2008) Identifying pathogenic genetic background of simplex or multiplex retinitis pigmentosa patients: a large scale mutation screening study. J Med Genet 45: 465–472.
12. Ikeda H, Osakada F, Watanabe K, Mizuseki K, Haraguchi T, et al. (2005) Generation of Rx+/Pax6+ neural retinal precursors from embryonic stem cells. Proc Natl Acad Sci U S A 102: 11331–11336.
13. Sung CH, Davenport CM, Nathans J (1993) Rhodopsin mutations responsible for autosomal dominant retinitis pigmentosa. Clustering of functional classes along the polypeptide chain. J Biol Chem 268: 26645–26649.
14. van Leeuwen R, Boekhoorn S, Vingerling JR, Witteman JC, Klaver CC, et al. (2005) Dietary intake of antioxidants and risk of age-related macular degeneration. JAMA 294: 3101–3107.
15. van Helden YG, Keijer J, Heil SG, Picó C, Palou A, et al. (2009) Beta-carotene affects oxidative stress-related DNA damage in lung epithelial cells and in ferret lung. Carcinogenesis 30: 2070–2076.

One case of peripheral ulcerative keratitis (Leroux et al. 2004) and one case of paralimbal keratitis caused by candida glabrata (Djalilian et al. 2001) have been reported in patients with CGD. However, no case with so centrally positioned infiltrate and such deterioration of BCVA has been reported. The negative culture can be interpreted as noninfectious infiltrate in the left cornea, but the profound clinical and subjective improvement after the prescription of levofloxacin drops implies the opposite. The fact that antibiotic drops were prescribed 2 days earlier can perhaps explain the negative culture, as this can interfere with microbiology testing. The other possibility but less likely would be a sterile inflammatory keratitis (maybe related to granuloma formations already known in other organs), which has not been described earlier in such patients. Regarding other possible systemic causes of granulomas, the patient has regular contact with infection clinic, and no other infections have been diagnosed.

References

Djalilian AR, Smith JA, Walsh TJ, Malech HL & Robinson MR (2001): Keratitis caused by Candida glabrata in a patient with chronic granulomatous disease. Am J Ophthalmol **132**: 782–783.

Goldblatt D, Butcher J, Thrasher AJ & Russell-Eggitt I (1999): Chorioretinal lesions in patients and carriers of chronic granulomatous disease. J Pediatr **134**: 780–783.

Johnston RB Jr (2001): Clinical aspects of chronic granulomatous disease. Curr Opin Hematol **8**: 17–22.Review.

Kim SJ, Kim JG & Yu YS (2003): Chorioretinal lesions in patients with chronic granulomatous disease. Retina **23**: 360–365.

Leroux K, Mallon E & Ayliffe WH (2004): Chronic granulomatous disease and peripheral ulcerative keratitis: a rare case of recurrent external ocular disease. Bull Soc Belge Ophtalmol **293**: 47–53.

Correspodence:
Dr Marios Panagiotopoulos
Department of Ophthalmology
Örebro University Hospital
70185 Örebro
Sweden
Tel: + 46 19 6021000
Fax: + 46 19 6021052
Email: marios.panagiotopoulos@orebroll.se

Stargardt Disease with Preserved Central Vision: identification of a putative novel mutation in ATP-binding cassette transporter gene

Kaoru Fujinami,[1] Masakazu Akahori,[2] Masaki Fukui,[1] Kazushige Tsunoda,[1] Takeshi Iwata,[2] and Yozo Miyake[1,3]

[1]Laboratory of Visual Physiology, National Institute of Sensory Organs, Meguro-ku, Tokyo, Japan
[2]Division of Molecular & Cellular Biology, National Institute of Sensory Organs, National Hospital Organization, Tokyo Medical Center, Meguro-ku, Tokyo, Japan
[3]Aichi Shukutoku University, Aichi, Japan, Nagakute-cho, Aichi-gun, Aichi, Japan

doi: 10.1111/j.1755-3768.2009.01848.x

Editor,

Stargardt disease (STGD) has a juvenile to young–adult onset, a rapid decrease of central vision and a progressive bilateral atrophy of the sensory retina and retinal pigment epithelium (RPE) in the macula. Yellow-orange flecks are often detected around the macula, the midretina and or both (Rotenstreich et al. 2003). Mutations in the gene encoding the ATP-binding cassette transporter gene (ABCA4) are responsible for autosomal recessive STGD (Allikmets 1997; Webster et al. 2001). We examined a patient who had the characteristic signs of STGD but had good visual acuity.

A 66-year-old man complained of photophobia and a paracentral scotoma which was present since his teens and had not worsened. None of his family members had similar symptoms. His visual acuity was 20/15 OU, and ophthalmoscopy identified a dark brown, well-demarcated area at the fovea surrounded by RPE atrophy and flecks (Fig. 1A). Fluorescein angiography showed window defects at the flecks and a dark choroid (Fig. 1B). The optical coherence tomographic (OCT) images showed a well-preserved sensory retina and normal thickness RPE at the fovea (Fig. 1C, D). The foveal area was surrounded by atrophic sensory retina and RPE. Static perimetry showed ring-shaped paracentral relative scotoma which surrounded the normal area seeing area of 5° (Fig. 1E). Focal macular electroretinograms (FMERGs) also demonstrated a well-preserved retinal function at the fovea (Fig. 1F). Compared to age-matched controls, the FMERGs had normal responses elicited by a 5-degree stimulus spot and severely reduced responses elicited by 10-degree and 15-degree spots (Fig. 1F, G). Genetic analysis with direct DNA sequencing of amplified products revealed four reported polymorphisms (Allikmets 1997; Briggs et al. 2001; Webster et al. 2001; Fukui et al. 2002) and one novel mutation, Met280Thr, in exon 7 of the ABCA4 gene (Table 1).

Our patient had clinical findings that were pathognomonic of typical STGD, except that the clinical course was stationary and he had 20/15 vision because of well-preserved foveal function. The preserved foveal area was small and well demarcated. Visual acuity, fundus appearance, OCT images, static perimetry and FMERGs supported the well-preserved foveal function. We report our case because the patient had a unique phenotype with a novel putative mutation in the *ABCA4* gene, not yet shown to segregate with the disease.

The well-demarcated dark brown foveal RPE appeared to be hyperpigmented although the thickness measured by OCT was 29 μm which was within normal limits. The findings in our case could indicate that the non-atrophic foveal RPE had an effect in preserving the foveal morphology and function.

The inheritance of STGD is autosomal recessive; however, our patient had four polymorphisms and one heterozygous gene mutation c.839T > C in exon 7 in the *ABCA4* gene. A second mutation was not found, but it may well exist outside of the coding sequence of the *ABCA4* gene. The new mutation in our patient was located outside the known functional domains of ATP-binding or transmembrane site (Lewis et al. 1999), which may explain the mild effect of the missense mutation. We should